TNO Physics and Electronics Laboratory

TNO Defence Research

AD-A285 347

TD 94-1395

0

TNO-report FEL-94-B195

copy no.: 8

title:

Diffraction computation by means of the Method of Equivalent Currents

TD 94-1395

TNO Defence Research

TNC
Labo TD 94-1395

Oude Waalsdorperweg 63
2597 AK The Hague
P.O. Box 96864
2509 JG The Hague
The Netherlands

Fax +31 70 328 09 61
Phone +31 70 326 42 21

TNO-report
FEL-94-B195

copy no.: 8

title:

Diffraction computation by means of the Method of Equivalent Currents

author(s):

L.J. van Ewijk

date:

July 1994

classification

classified by	:	H.R. van Es
classification date	:	May 1994
title	:	Ongerubriceerd
managementuittreksel	:	Ongerubriceerd
abstract	:	Ongerubriceerd
report text	:	Ongerubriceerd
appendices A - C	:	Ongerubriceerd

no. of copies	:	27
no. of pages	:	43 (incl. appendices, excl. RDP & distribution list)
no. of appendices	:	3

All information which is classified according to Dutch regulations shall be treated by the recipient in the same way as classified information of corresponding value in his own country. No part of this information will be disclosed to any party.
The classification designation Ongerubriceerd is equivalent to Unclassified, Stg. Confidentieel is equivalent to Confidential and Stg. Geheim is equivalent to Secret.

MANAGEMENTUITTREKSEL

titel	:	Diffraction computation by means of the Method of Equivalent Currents
auteur(s)	:	L.J. van Ewijk
datum	:	juli 1994
opdrachtnr.	:	-
IWP-nr.	:	760.3
rapportnr.	:	FEL-94-B195

Dit rapport is het eerste van een serie van 3 rapporten over diffractierekening met behulp van hoogfrequent technieken. Het werk waarover in deze rapporten verslag wordt gedaan is verricht door L.J. v. Ewijk tijdens zijn detachering bij het Defense Research Establishment Ottawa (DREO) in Canada van september 1992 tot en met augustus 1993. Het werk heeft daar onder andere geleid tot de ontwikkeling van drie codes die gebruikt kunnen worden op het gebied van RCS berekening.

Dit rapport geeft een afleiding van een veelbelovende diffractietechniek uit de literatuur. De reden dat deze afleiding hier gegeven wordt, terwijl deze ook in de literatuur te vinden is, is dat de afleiding in de literatuur verspreid is over verscheidene artikelen en hier integraal gegeven wordt. Bovendien worden hier enkele singulariteiten nader beschouwd, en verholpen, terwijl dat in de literatuur niet het geval is. Zonder een volledig inzicht in de afleiding is deze singulariteitenanalyse niet eenvoudig te volgen.

De totale afleiding is weergegeven in een bijlage. De hoofdtekst van het rapport bevat een inzichtelijk overzicht van de methode, een vergelijking met gemeten resultaten en de conclusies die uit deze vergelijkingen kunnen worden getrokken.

In het algemeen kan worden gesteld dat de gekozen methode goed voldoet en de gebruikelijke reflectieberekeningen sterk kan verbeteren. Dit is vooral zo in het geval van verstrooiing aan scherpe randen waarbij de invalsrichting van het veld loodrecht staat op de rand. Bij schuine inval is de invloed van het berekende diffractieveld minder sterk.

De combinatie van hoogfrequent rekenmethoden die in dit rapport wordt behandeld is in staat om voor vele situaties de radardoorsnede van objecten te berekenen. Voor die gevallen waar, volgens de vergelijkingen met meetresultaten die in dit rapport gepresenteerd worden, de methode nog tekort schiet wordt aangegeven wat een mogelijke verbetering zou kunnen zijn. Deze bestaat uit het simuleren van de "surface travelling wave" door het meermalen toepassen van de diffractiemethode. De implementatie hiervan wordt in de overige twee rapporten, zoals hierboven vermeld, behandeld.

Het in dit rapport beschreven werk heeft geleid tot beter inzicht in de fysische achtergronden van het verstrooiingsproces aan scherpe randen, de verbetering van een van de meest veelzijdig toepasbare diffractietechnieken en de implementatie van deze methode in een rekenprogramma. Met dit rekenprogramma is het nu mogelijk om de diffractie aan scherpe randen te berekenen voor bijna alle invals- en observatierichtingen. Slechts één richting vertoont nog een singulier gedrag, hetgeen problemen oplevert als men het verstrooide veld wil berekenen in de richting

van de voortzetting van de invallende straal langs een van de oppervlakken van de wig indien die invallende straal van buiten de wig komt.
De toegevoegde waarde van de berekening van diffractieverschijnselen ten opzichte van uitsluitend reflectieverschijnselen komt het best tot uiting bij de analyse van objecten met lage radardoorsnede. De hierboven genoemde uitbreiding zal deze toegevoegde waarde nog doen toenemen.

CONTENTS

1 INTRODUCTION

The Method of Equivalent Currents (MEC) finds its origin in the fact that any finite current distribution yields a finite result for the scattered field when that contribution is summed in the radiation integral [1]. So, when the proper current distribution can be found, the problems with axial caustics, as in the Geometrical Theory of Diffraction (GTD), can be avoided. Furthermore, by using equivalent currents it is possible to determine the scattered field outside the directions defined by the Keller cone.

The approach in the MEC currents is to assume the existence of filamentry electric and magnetic surface currents in the neighbourhood of surface discontinuities, such as edges, and to add these currents to the far-field radiation integral. It is emphasised here that the equivalent currents are not to be confused with real physical currents. They are not really present at the edge, but are merely a mathematical aid to correctly represent the scattered field. This is clear when we notice for instance that these currents are dependent on the observation direction, which is impossible for physical currents.

An overview of the MEC can be found in [1]. The method is used by many authors, see for instance Millar [2], [3] and [4], Ryan and Peters [5], Knott and Senior [6] and Sikta [7]. In these articles the MEC is used for various scattering problems and in some of them the results are compared to the results of other techniques.

Knott and Senior [6] adjusted the equivalent current prescription by requiring that a stationary phase evaluation of the radiation integral yields the GTD result for directions on the Keller cone. In order to extend the expressions to general bistatic conditions they replaced some terms to invoke dependency on the incidence and observation direction, a method later criticised by Michaeli [8].

Sikta [7] used the equivalent currents for flat plates which he divided in strips with width that approached zero.

Michaeli [8] and [9] proposed a more rigorous way to derive expressions for the equivalent currents. He stated that the usual expressions were based on GTD-like expressions and were therefore only valid for directions on the Keller cone. He then derived new expressions based on the identification of the MEC line integral with the asymptotic edge contribution to the Physical Theory of Diffraction (PTD) surface integral. From this resulted the equivalent currents expressed in terms of the PTD surface currents. These integrals were then evaluated, resulting in the equivalent currents that could be used to determine the scattered field by an arbitrary edge [8]. Later he improved his expressions by using a different integration variable in the evaluation of the afore mentioned integrals [9]. He also split his equivalent currents into fringe equivalent currents, accounting for the fringe scattered field, and Physical Optics (PO) equivalent currents, accounting for the PO scattered field. The fringe currents, or non-uniform currents as they were named originally by Ufimtsev, are defined as the difference between the total currents on a surface and the PO currents [10]. The step to split the equivalent currents into fringe equivalent currents and PO equivalent currents was initiated by Knott [11]. He had compared the equivalent currents with the method of Incremental Length Diffraction Coefficients (ILDC), derived by Mitzner in 1974. Knott pointed out that the difference between MEC and ILDC was caused by the fact that Michaeli used the total surface currents and Mitzner the non-uniform currents only, so their results differ by terms due to the PO currents. Although Mitzner derived his theory in

1974, his report was only available in limited distribution for a long time, so Michaeli and Mitzner reached their results independently.

Because the equivalent currents are now known as fringe equivalent currents and PO equivalent currents they are very suitable to use in a high-frequency Radar Cross Section (RCS) prediction program. We can for instance always apply the PO integral to an object of which we want to determine the RCS but only apply the method of equivalent currents to those edges that are expected to give a significant contribution to the total scattering. This last step can decrease the computational time considerably because a calculation using equivalent currents is far more computation intensive than using PO. It also implies, however, that a priori knowledge is necessary to decide whether an edge gives a significant contribution or not and such knowledge is not always available.

In chapter 2 the method of equivalent currents is rederived following Michaeli [8], [9] and casted in a form comparable to other techniques and with the same variables as used in other reports. Chapter 3 will show some results obtained with the computer program in which the MEC is implemented compared to measurement results.

The work described in this report has been done while the author was at the Defence Research Establishment Ottawa (DREO) in the framework of the Canadian Defence Research Fellowship Program. The author had his office at the David Florida Laboratory of the Canadian Space Agency, where much of this kind of work is done for DREO, and was guided by Dr. S. Mishra. The measurements that are used for the comparisons in chapter 3 are done at the DDARLING facility at DFL by C. Larose.

2 THE METHOD OF EQUIVALENT CURRENTS

As mentioned in the introduction this chapter contains a derivation of the equivalent currents, following the way Michaeli did.
This is done by identifying the non-uniform currents, known from the PTD, with a magnetic and electric current flowing at the edge under consideration. An expression can then be found for these currents after which they will be used in the radiation integral in order to compute the scattered field. This will only be the edge-diffracted field because the uniform part of the induced total currents is omitted explicitly from these expressions. When one wants to compute the total scattered field one has to add the contribution to this field by the uniform currents, for instance by means of a PO computation.

2.1 The equivalent currents

In the following we use the co-ordinates and angles as shown in figure 2.1. The suffixes to the angles are 1 and 2, instead of i and s, because they are related to one of the planes of the wedge. The suffixes i and s ususally denote angles related to the co-ordinate axes. When the edge is aligned with the z-axis these angles are equal, but generally they are not.
When the suffixes 1 and 2 are used in conjunction with any other parameter they denote the facenumber that the parameter is related to.

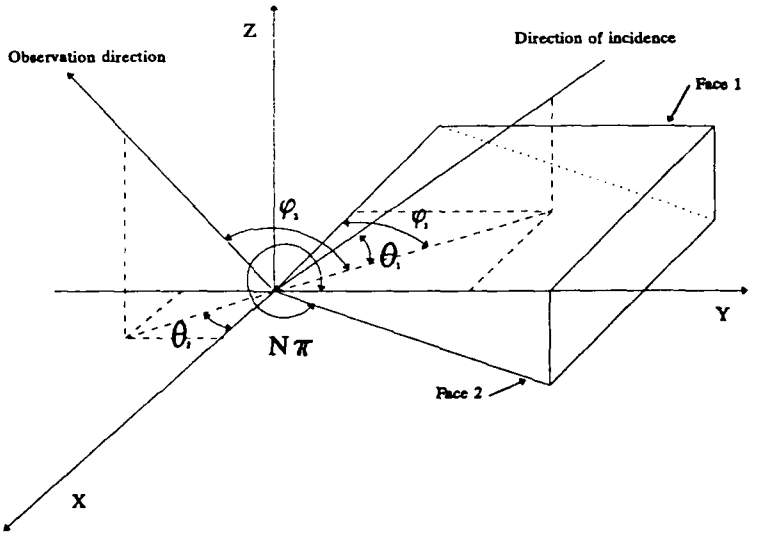

Fig 2.1: *The general configuration of the wedge used to determine the equivalent currents. The angles shown in this picture are related to one of the planes that compose the wedge. The faces are numbered 1 and 2.*

When we assume electric and magnetic currents flowing along an edge C we can determine the scattered field caused by these currents from the radiation integral, see for instance [13] or [14]:

$$\bar{E}_d = ik\sqrt{\frac{\mu}{\varepsilon}}\int_C \left[(\bar{I}_e \cdot \hat{k}_s)\hat{k}_s - \bar{I}_e - \sqrt{\frac{\varepsilon}{\mu}}\bar{I}_m x\hat{k}_s \right] \psi(\bar{r}', \bar{r})dl' \qquad (1)$$

where the vector I denotes an equivalent current, as opposed to J, a physical current. In this equation only integration along the edge is necessary because this is the only source for the currents. This equation can also be expressed as:

$$\bar{E}_d = ik\sqrt{\frac{\mu}{\varepsilon}}\int_C \left[I_e \hat{k}_s x(\hat{k}_s x\hat{t}) + \sqrt{\frac{\varepsilon}{\mu}} I_m \hat{k}_s x\hat{t} \right] \psi(\bar{r}', \bar{r})dl' \qquad (2)$$

where the unit vector t denotes the direction of the edge under consideration and I_e and I_m are now complex numbers instead of vectors. The equivalent currents are always directed along the edge.
We also know that the scattered field can be expressed in terms of the physical currents as:

$$E_s = ik\sqrt{\frac{\mu}{\varepsilon}}\sum_{n=1}^{2}\iint_{S_n} J_n \hat{k}_s x(\hat{k}_s x\hat{t})\psi(r', r)dS \qquad (3)$$

for a perfectly conducting wedge. The summation in eq (3) is taken over both faces of the wedge.
Eq. (3) can be reduced, in the high frequency limit, asymptotically to a sum of ray field contributions from isolated stationary phase points and a boundary contribution expressed by a line integral along C. This latter integral should then be identified with eq (2).
We will assume that the edge diffraction is caused by surface currents on narrow strips, S_1 and S_2, along C. Let σ_1 and σ_2 be the vectors from C, perpendicular to C in the direction of the grazing diffracted ray on face 1 and 2 respectively, see figure 2.2.

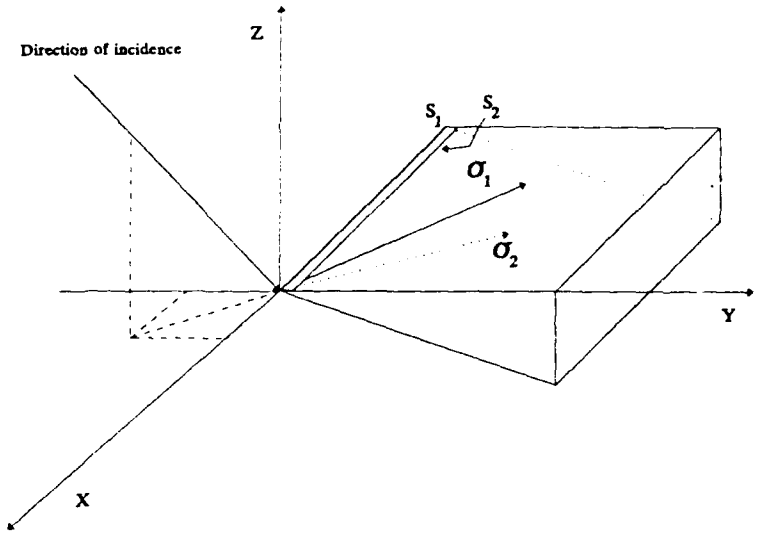

Fig 2.2: *The direction of the grazing diffracted ray is denoted by σ_1 or σ_2, the area where the equivalent currents flow is denoted by S_1 or S_2 (Note that S_2 actually is not visible). The suffix (1 or 2) to these parameters, indicate the corresponding plane of the wedge, see fig 2.1.*

We then write this integral in such a way that only the asymptotic endpoint contribution for the σ-integration is taken into account, i.e. the contribution at σ=0, so the edge. Green's function can be approximated by this function evaluated at the edge multiplied by $\exp(ik\sigma_i \cdot k_s)$. This gives for the edge diffracted part of the scattered field from eq (3):

$$\vec{E}_d = ik\sqrt{\frac{\mu}{\varepsilon}}\int_C \sum_{n=1}^{2} \int \hat{k}_s x(\hat{k}_s x \vec{J}_n)\psi_e e^{ik\sigma_n \hat{k}_s} \sin(\theta_i) d\sigma_n dl \qquad (4)$$

where the summation is taken over the two faces of the wedge.
By comparing eq (2) and (4) and some vector calculus we can find expressions for the equivalent currents in terms of the integral of the current on the wedge. These currents are taken to be the fringe currents, or non-uniform currents, only. The solution is then found by an asymptotic end point evaluation of these integrals, by using the solution of the canonical wedge problem and theorems from complex function theory. This evaluation is done in Appendix A.
The result of this is given in eq(5) and (6):

$$I_m = \frac{2iZH_{iz}}{Nk\sin(\theta_1)\sin(\theta_2)}\{ \frac{N\sin(\varphi_2)U(\pi-\varphi_1)}{\cos(\varphi_1)+\mu_1} + \frac{N\sin(N\pi-\varphi_2)U((1-N)\pi+\varphi_1)}{\cos(N\pi-\varphi_1)+\mu_2} + \frac{\sin(\frac{\pi-\alpha_1}{N})}{\cos(\frac{\pi-\alpha_1}{N})-\cos(\frac{\varphi_1}{N})}\frac{\sin(\varphi_2)}{\sin(\alpha_1)} + \frac{\sin(\frac{\pi-\alpha_2}{N})}{\cos(\frac{\pi-\alpha_2}{N})+\cos(\frac{\varphi_1}{N})}\frac{\sin(N\pi-\varphi_2)}{\sin(\alpha_2)}\} \tag{5}$$

and

$$I_e = \frac{2i\sqrt{\frac{\varepsilon}{\mu}}E_{iz}}{k\sin^2(\theta_1)}\{-\frac{\sin(\varphi_1)U(\pi-\varphi_1)}{\cos(\varphi_1)+\mu_1} - \frac{\sin(N\pi-\varphi_1)U((1-N)\pi+\varphi_1)}{\cos(N\pi-\varphi_1)+\mu_2} - \frac{\sin(\frac{\varphi_1}{N})}{N}\left[\frac{1}{\cos(\frac{\pi-\alpha_1}{N})-\cos(\frac{\varphi_1}{N})}+\frac{1}{\cos(\frac{\pi-\alpha_2}{N})+\cos(\frac{\varphi_1}{N})}\right]\}$$
$$\frac{2iH_{iz}}{k\sin(\theta_1)}\{\frac{\cos(\theta_1)}{\sin(\theta_1)}\left[\frac{\cos(\varphi_1)U(\pi-\varphi_1)}{\cos(\varphi_1)+\mu_1} - \frac{\cos(N\pi-\varphi_1)U((1-N)\pi+\varphi_1)}{\cos(N\pi-\varphi_1)+\mu_2}\right] +$$
$$\frac{\sin(\frac{\pi-\alpha_1}{N})}{N}\frac{\sin(\alpha_1)}{\cos(\frac{\pi-\alpha_1}{N})-\cos(\frac{\varphi_1}{N})}\left[\frac{\mu_1}{\tan(\theta_2)}-\frac{\cos(\varphi_2)}{\tan(\theta_2)}\right]+$$
$$\frac{\sin(\frac{\pi-\alpha_2}{N})}{N}\frac{\sin(\alpha_2)}{\cos(\frac{\pi-\alpha_2}{N})+\cos(\frac{\varphi_1}{N})}\left[\frac{\mu_2}{\tan(\theta_1)}-\frac{\cos(N\pi-\varphi_2)}{\tan(\theta_2)}\right]\} \tag{6}$$

where μ is given in eq (A.11) as:

$$\mu = \frac{\sin(\theta_1)\sin(\theta_2)\cos(\varphi_2)+\cos(\theta_1)\cos(\theta_2)-\cos^2(\theta_1)}{\sin^2(\theta_1)} \tag{7}$$

and $\alpha=\arccos(\mu)$. These equations look very complex and cumbersome to use, but they only involve simple goniometric functions that cause no problems in a computer program. The arccos that must be calculated can sometimes result in a complex number, however, so care must be taken to use the correct expression for this, see Appendix C.

2.2 The diffracted field

With eq's (2), (5) and (6) we can compute the edge scattered field, or diffracted field, caused by the fringe currents. The radiation integral is easily solved, because the only dependency of I_e and I_m on r' is through the incident field. This term can be kept under the integral, while the other terms can be taken outside the integral. When writing the solution in terms of diffraction coefficients [12] we get:

$$\begin{aligned} I_e &= \frac{2iE_{iz}}{kZ\sin^2(\theta_i)} D_e + \frac{2iH_{iz}}{k\sin(\theta_i)} D_x \\ I_m &= \frac{2iZH_{iz}}{k\sin(\theta_i)\sin(\theta_2)} D_m \end{aligned} \tag{8}$$

with D_e, D_x and D_m as following from eq's (5) and (6). By using the radiation integral and expressing the incident field as we did in the derivation of Physical Optics, we find:

$$\begin{aligned} \vec{E} = \frac{ike^{-ikR_0}}{4\pi R_0} \{ \sqrt{\frac{\mu}{\varepsilon}} [\frac{2iE_{0iz}}{kZ\sin^2(\theta_i)} D_e + \frac{2iH_{0iz}}{k\sin(\theta_i)} D_x](\hat{k}_s x(\hat{k}_s x\hat{t})) + \\ \frac{2iZH_{0iz}}{k\sin(\theta_i)\sin(\theta_2)} D_m(\hat{k}_s x\hat{t}) \} \int_C e^{-ik(\hat{k}_i-\hat{k}_s)\vec{r}'} dl' \end{aligned} \tag{9}$$

The integral can be solved easily by using a parameter representation of the edge:

$$\begin{aligned} dl' &= \Delta a\, ds, \qquad 0 \le s \le 1 \\ \vec{r}' &= a_0 + s\,\Delta\vec{a} \end{aligned} \tag{10}$$

with a_0 the start point of the edge and Δa the vector along the edge with length equal to the edge. After evaluation we find:

$$I = \Delta a\ \mathrm{sinc}\left[k(\hat{k}_i - \hat{k}_s)\cdot\frac{\Delta\vec{a}}{2} \right] e^{-ik(\hat{k}_i-\hat{k}_s)(\vec{a}_0+\frac{\Delta\vec{a}}{2})} \tag{11}$$

During the evaluation of eq (11) we had to restrict ourselves to an observation direction away from the Keller cone. This restriction is only mathematical, however, and the sinc function in eq (11) ensures the correct result for these directions of observation as well.

Substitution of eq (11) in (9) and by omitting some terms which would cancel anyway when calculating the RCS results in:

$$\vec{E}_d = \frac{ik}{2\sqrt{\pi}}\{[\frac{2iE_{0iz}}{k\sin^2(\theta_1)}D_e + \frac{2iZH_{0iz}}{k\sin(\theta_1)}D_x](\hat{k}_s x(\hat{k}_s x\hat{t})) + \frac{2iZH_{0iz}}{k\sin(\theta_1)\sin(\theta_2)}D_m(\hat{k}_s x\hat{t})\}$$
$$\Delta a\,\mathrm{sinc}[k(\hat{k}_i - \hat{k}_s)\cdot\frac{\Delta\vec{a}}{2}]e^{-ik(\hat{k}_i-\hat{k}_s)(\vec{a}_n+\frac{\Delta\vec{a}}{2})} \qquad (12)$$

2.3 Singularities in the diffraction coefficients

From eq (5), (6) and (8) the diffraction coefficients can be found easily. Also, some singularities in these expressions can be pointed out. This is done in Appendix B where the way to circumvent these singularities is described as well. One of the mentioned singularities will be shown here as well, as an example.
From the expression for D_m we can find that this coefficient becomes singular when:

$$\begin{aligned}
&\cos(\varphi_1) = -\mu_1 \\
&\cos(N\pi - \varphi_1) = -\mu_2 \\
&\cos(\frac{\pi-\alpha_1}{N}) = \cos(\frac{\varphi_1}{N}) \\
&\cos(\frac{\pi-\alpha_2}{N}) = -\cos(\frac{\varphi_1}{N})
\end{aligned} \qquad (13)$$

When the observation direction is on the Keller cone [1], these singular directions coincide with the shadow and reflection boundaries of face 1 and face 2 of the wedge respectively, see Appendix B. When the observation direction is outside the Keller cone the singularities occur as well, however, so it is not possible to change to different diffraction coefficients, which would be the easiest solution.
The way to prevent these singularities is by evaluating D_m when μ_1 approaches the value given by eq (13) infinitely close. This evaluation is given in Appendix B for all singularities, given by eq (13), as well as for all the singularities in D_e and D_x. The resulting expressions are used in the developed computer program whenever the combination of incidence and observation direction is chosen such that the coefficient would become singular.
After the removal of these singularities only one singularity will remain. This is called the Ufimtsev singularity by Michaeli [8] and it only occurs when computing forward scattering. This singularity will therefore only rarely pose problems when calculating RCS.

3 COMPARISON OF COMPUTED AND MEASURED RESULTS

With the computer program that applies the MEC as derived in chapter 2 it is possible to compute the diffracted field of general edges. These edges must be defined in a suitable way of course, but there is no restriction on the external wedge angle of the edge. Any value between 0 and 2π can be used. The diffracted field can be computed as function of aspect angle, frequency or bistatic angle. The edge is assumed to be perfectly conducting.
To show the capabilities of the method a set of objects is chosen for which measured data was made available. The improvement by the MEC on the scattering computation by PO will be made clear as will the shortcomings of a single diffraction theory in general.
The objects used for this analysis are:

- square plate
- square rod
- equilateral triangular plate
- pyramid
- circular cylinder

The size of the objects is such that they can be treated by high-frequency methods in the frequency range that is used in the measurement facility at DFL.
The graphs shown in this chapter display RCS values as function of the incident angle, usually the azimuth angle. The vertical axis displays the RCS in dB m^2, the horizontal axis displays the incident angle. The scale that is chosen to be consistent for each object under consideration so the various results for any object can be compared easily. The pictures always contain 3 graphs, PO results only, PO+MEC results and measured data respectively.
The co-ordinate system as used in the computations is shown in fig 3.1. When the orientation of the objects is discussed in the next sections, the axes as shown in this figure will be referred to.

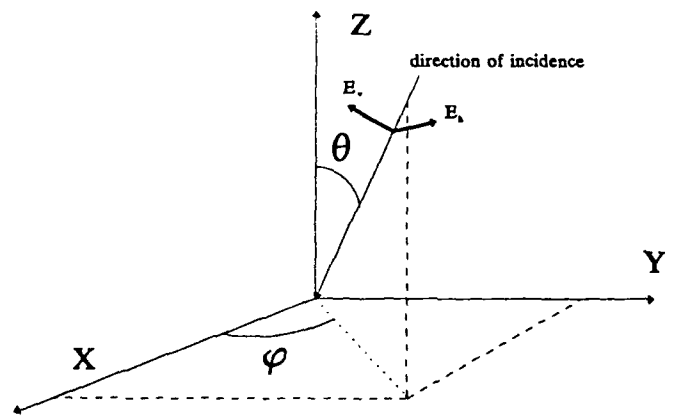

Fig 3.1: *The co-ordinate system as used for the computations in this chapter. The angles θ and φ denote the spherical co-ordinates and are used as elevation angle and azimuth angle respectively. In case of vertical polarisation, the electric field vector is directed as E_v, in case of horizontal polarisation as E_h.*

In fig 3.1 the x-, y- and z-axis are given as a right-hand co-ordinate system. With horizontal polarisation is meant that the electric field vector is perpendicular to the direction of incidence

and the z-axis, E_h in fig 3.1. Vertical polarisation indicates that the electric field vector is directed perpendicular to the direction of incidence and E_h, as shown by E_v in fig 3.1.

3.1 Square plate

The square plate used in this section has a sidelength of 17.78 cm (7") and measurements have been performed using various frequencies, from 5 to 18 GHz and for both linear polarisations.
Results for 5 GHz and 10 GHz will be shown, also for both linear polarisations, displaying the capability of the high-frequency methods to compute results over a wide frequency range. For the lowest frequency used the plate only is about 3λ by 3λ, just within the high-frequency region. The reason that no measured results are given at a higher frequency than 10 GHz is that the plate is not completely in the far field anymore at those frequencies, which would distort the comparison.
During measurements and computations the plate is located in the yz-plane with its vertical edges in the direction of the z-axis.

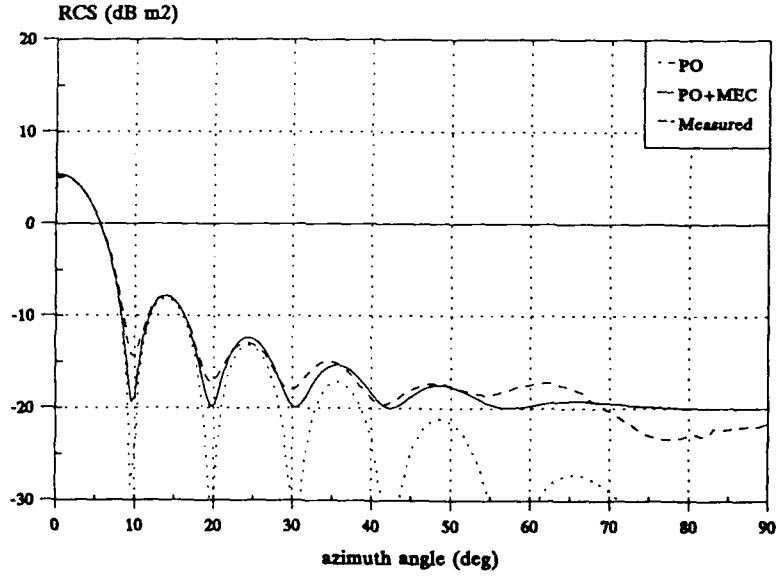

Fig 3.2: Measured and computed results for a square plate. Frequency used is 5 GHz, polarisation is V-V. The variable parameter in this case is the azimuth angle.

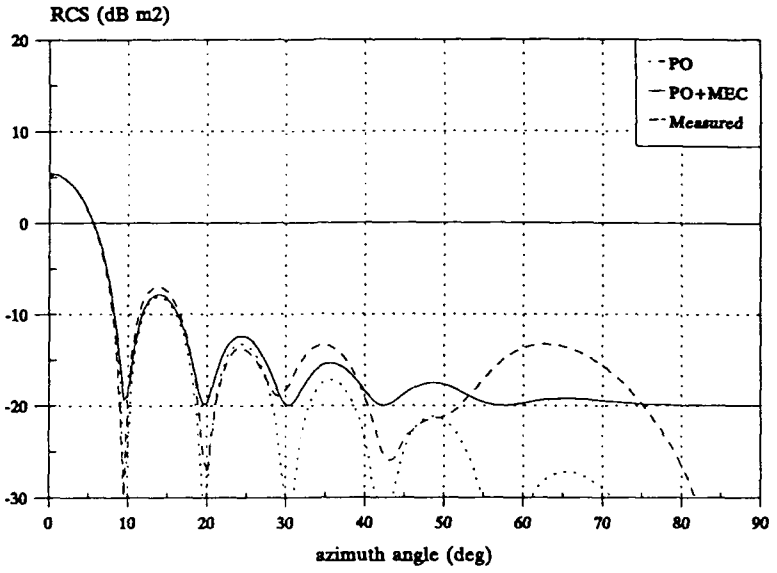

Fig 3.3: *Measured and computed results for the square plate. Frequency used is 5 GHz, polarisation is H-H.*

When comparing fig 3.2 and fig 3.3 it immediately becomes clear that the computed results for PO and MEC don't show any dependency on polarisation. This phenomenon is known for PO for all objects. The MEC only displays this kind of behaviour when applied to a flat plate, in all other cases different results will be found for the two linear polarisations. The measured data shows a broad and relatively high lobe at near grazing incident angles for horizontal polarisation. This lobe is caused by a travelling wave, see [1], a high-frequency scattering phenomenon that cannot be modelled accurately by any single diffraction theory.

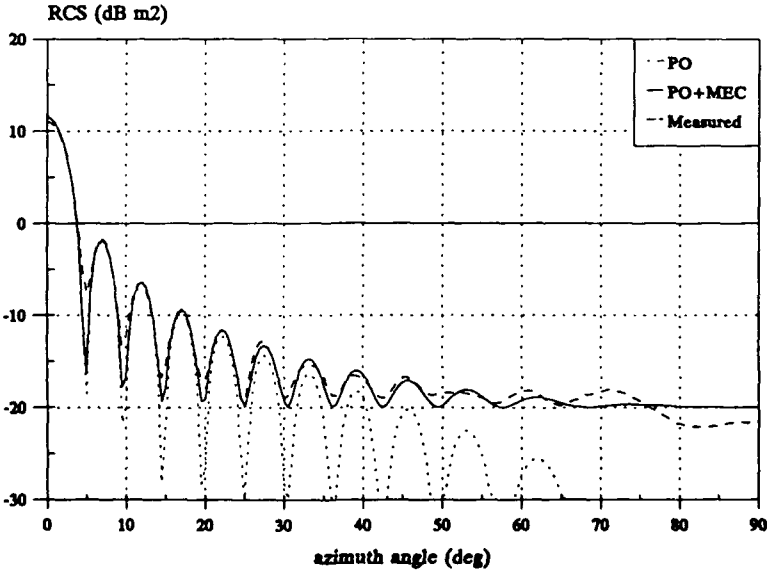

Fig 3.4: *Measured and computed results for the square plate. Frequency used is 10 GHz, polarisation is V-V.*

Fig 3.4 shows a comparison of a computation with PO and MEC with measured data at a frequency of 10 GHz. The size of the plate, 6 λ for this frequency, assures us to be well in the high-frequency region. Therefore, the computed results compare better to the measured data than they did in fig 3.2. The computational result of PO+MEC differs only a few dB from the measured data at maximum.

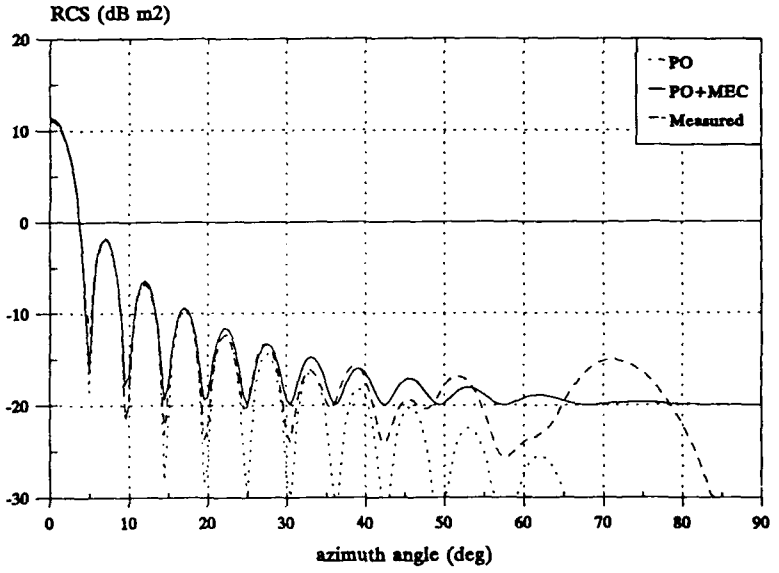

Fig 3.5: Measured and computed results for the square plate. Frequency used is 10 GHz. polarisation is H-H.

Fig 3.5 shows a similar deviation in the results of the computations, when compared to the measured result, at low grazing angles as fig 3.3. Again this difference is caused by the travelling wave. Despite this rather large defect the improvement of applying PO+MEC instead of PO alone is obvious.

3.2 Square rod

In this paragraph the measured and computed results for a square rod are given. Comparisons between results for 5 GHz and 15 GHz and for both linear polarisations will be given. Again, like in the case of the square plate, all dimensions are chosen similar for all pictures so as to ease the comparison. The size of the square rod is 7.1 cm by 7.1 cm by 17.78 cm (2.8" x 2.8" x 7"). Although it is not clear from the presented results it is noted that the measurements are performed with the rod lying down whereas the computations are performed with the rod standing upright. A difference that only results in the two linear polarisations being changed from measurement to computation. The plots show the results as function of elevation angle (note that this is related to the computations), so at 0° incident angle the top of the rod is illuminated perpendicularly.

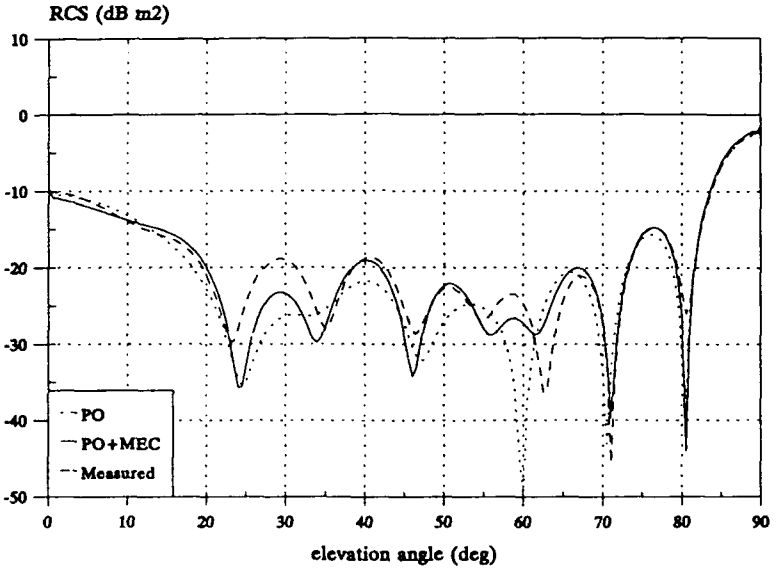

Fig. 3.6: *Measured and computed results for the square rod. Frequency used is 5 GHz, polarisation is V-V.*

In figure 3.6 we can see that, although the top of the rod only measures 1λ squared, the high-frequency techniques predict the RCS at these incident angles remarkably well. At higher incident angles some deviation is noticeable, up to 5 dB at a peak level, but just as we saw before, the MEC improves the PO prediction at those incident angles where PO shows large discrepancies.

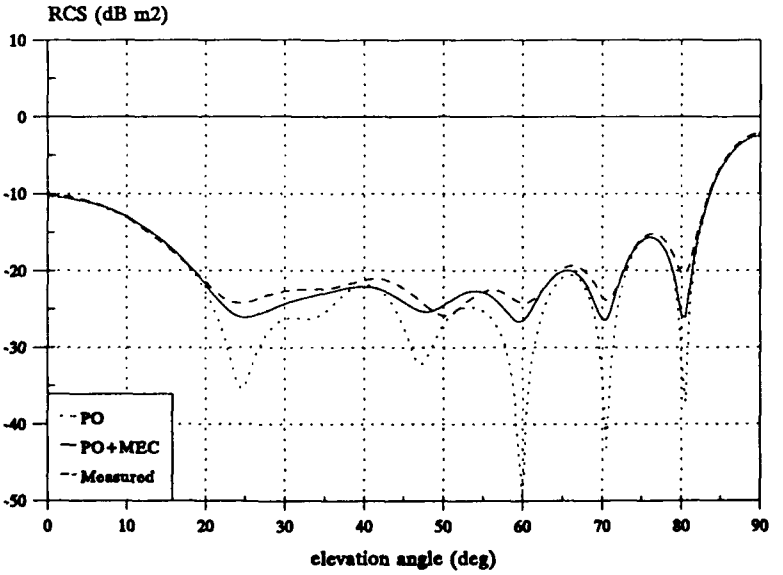

Fig 3.7 *Measured and computed results for the square rod. Frequency used is 5 GHz, polarisation is H-H.*

In the case of horizontal polarisation, fig 3.7, the usual lobe structure, that is found in almost all RCS plots of simple shapes, is absent in the measured data. The difference between the PO and PO+MEC result shows that the MEC takes care of the removal of this lobe structure that is, of course, present in the PO result. It can easily be understood that, especially in the low incident angle region, MEC has a large influence on the total result, because a leading edge is illuminated by an electromagnetic field with its electric filed vector directed along the edge. This shows in fig 3.7 as well.

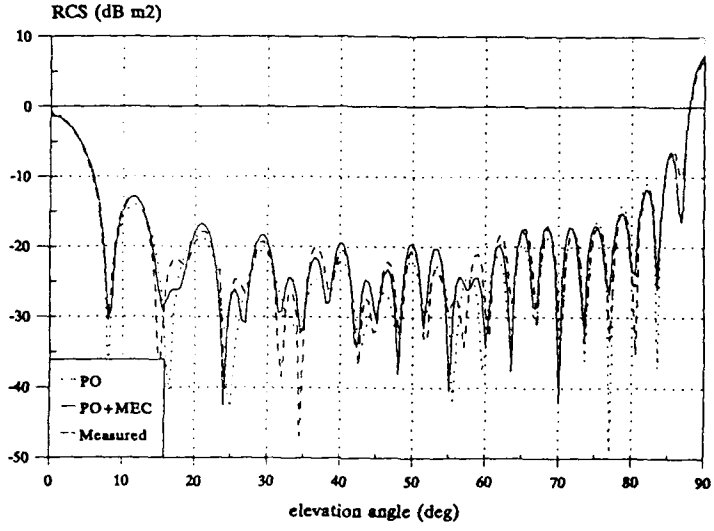

Fig 3.8: *Measured and computed results for the square rod. Frequency used is 15 GHz, polarisation is V-V.*

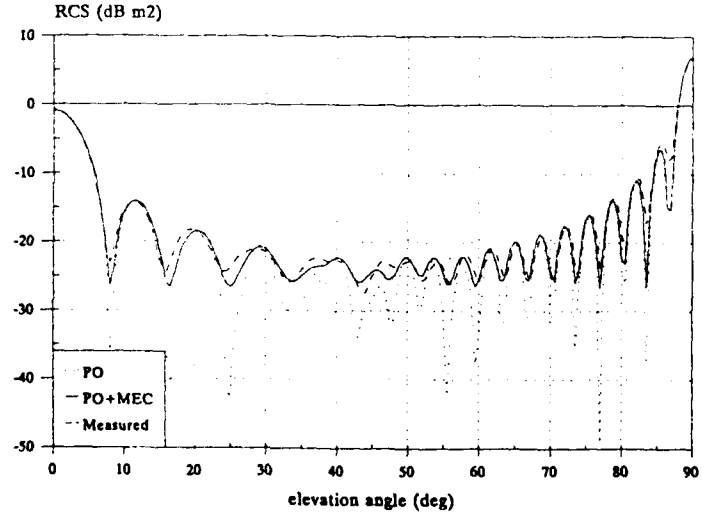

Fig 3.9: *Measured and computed results for the square rod. Frequency used is 15 GHz, polarisation is H-H.*

Figures 3.8 and 3.9 are similar comparisons as 3.6 and 3.7. The frequency used now is 15 GHz, so we can be sure the use of high-frequency methods is valid. This is clear as well from the results. MEC improves on PO as it did before. The eye-catching difference in lobing structure between fig 3.8 and 3.9 is again caused by the surface travelling wave, as explained in section 3.1. Note that the MEC, although it doesn't take into account this surface travelling wave, predicts the RCS reasonably well.

3.3 Equilateral triangular plate

The equilateral triangular plate in this section has a side length of 17.78 cm (7") and is located in the yz-plane during measurements and computations. Results are presented for 5 GHz and 15 GHz for both linear polarisations.

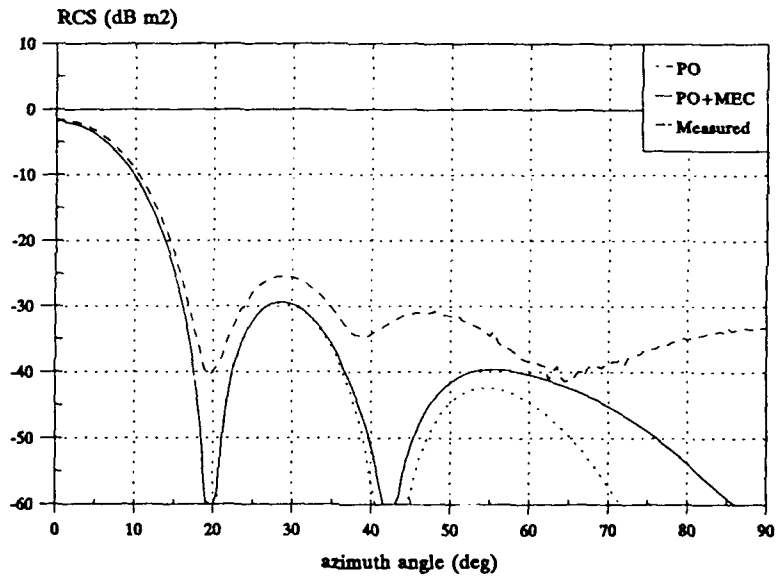

Fig 3.10: Measured and computed results for the equilateral triangular plate. Frequency used is 5 GHz, polarisation is V-V

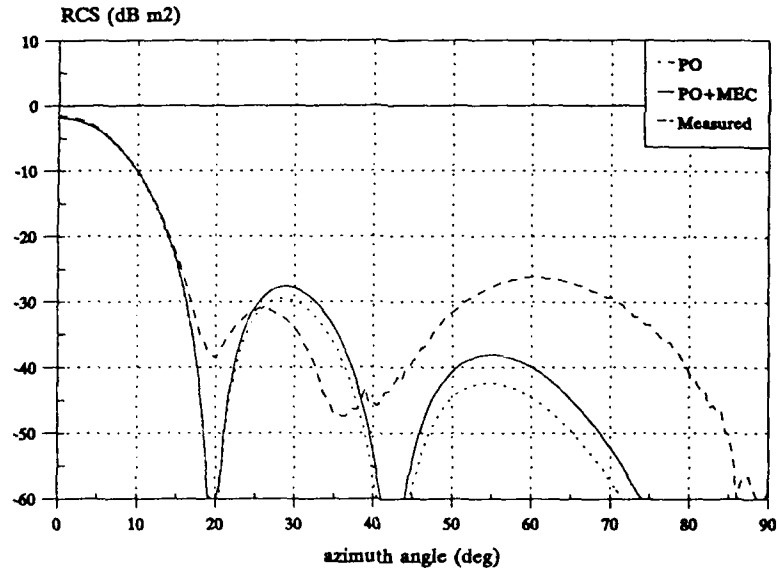

Fig 3.11: *Measured and computed results for the equilateral triangular plate. Frequency used is 5 GHz, polarisation is H-H.*

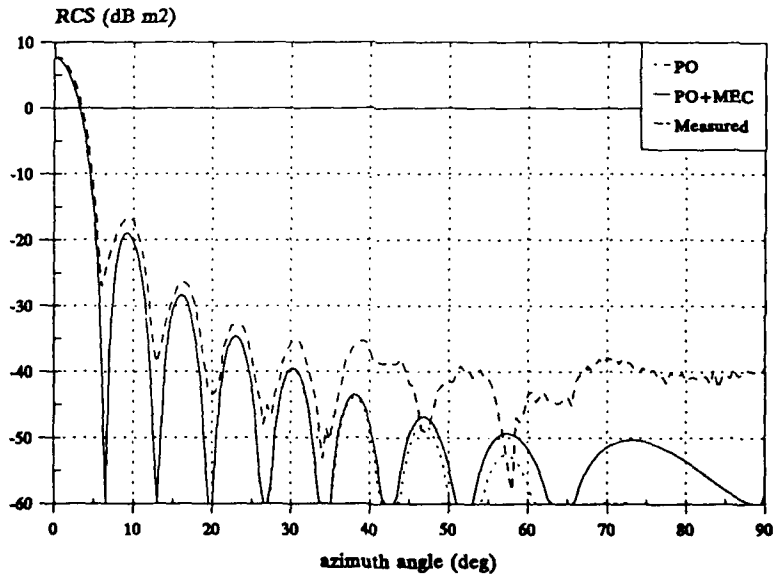

Fig 3.12: *Measured and computed results for the equilateral triangular plate. Frequency used is 15 GHz, polarisation is V-V.*

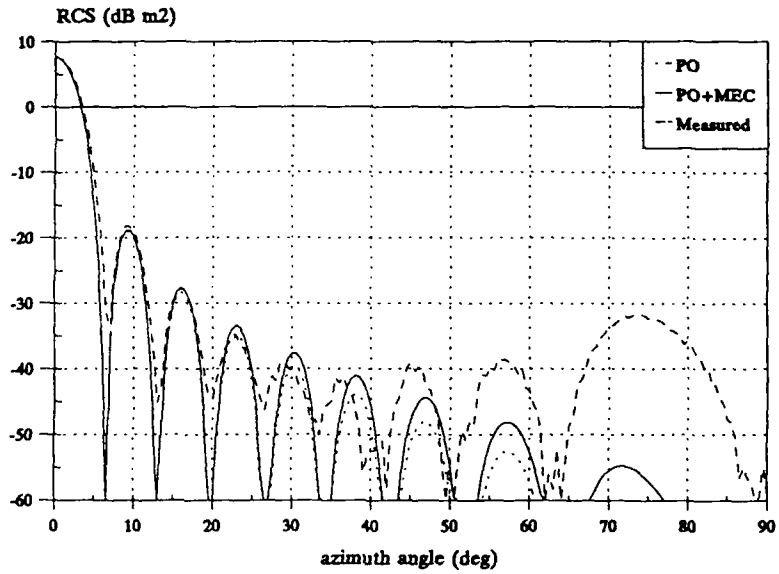

Fig 3.13: Measured and computed results for the equilateral triangular plate. Frequency used is 15 GHz, polarisation is H-H.

For the lower as well as the higher frequency the MEC doesn't influence the total result as much as it did in the results presented in the sections above. A reason for this might be the fact that the edges at which the field diffracts are slanted, as opposed to upright as they were before, which decreases the magnitude of the diffracted field. The results for H-H polarisation, fig 3.11 and 3.13, emphasise the need for a method to compute the surface travelling wave.

3.4 Pyramid

The pyramid that is considered in this section has a base length of 10 cm and the angle between the faces and the bottom is 40°. This makes the height approximately 4 cm. Because measurement results are only available at 10 GHz, this means that the pyramid does not fulfil the high-frequency requirements.
The bottom of the pyramid was placed in the xy-plane with the tip pointing towards the positive z-axis.

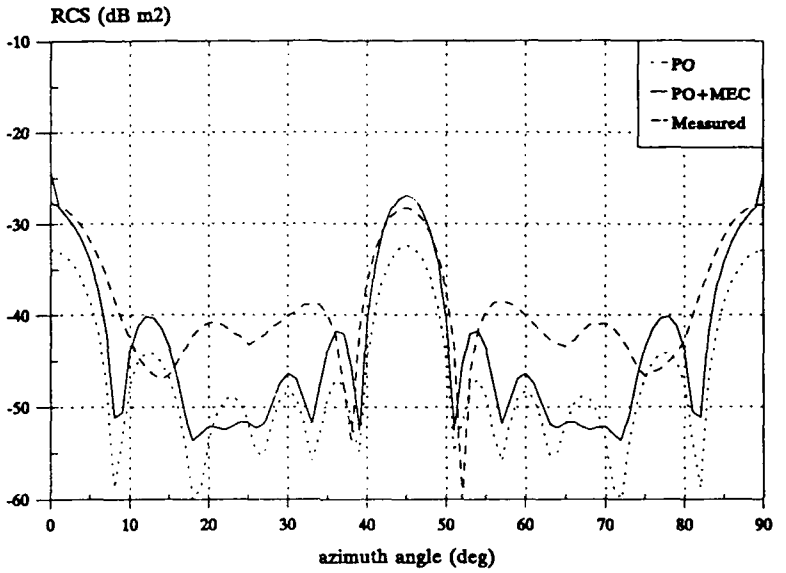

Fig 3.14: *Measured and computed results for the pyramid. Frequency used is 10 GHz, polarisation is V-V.*

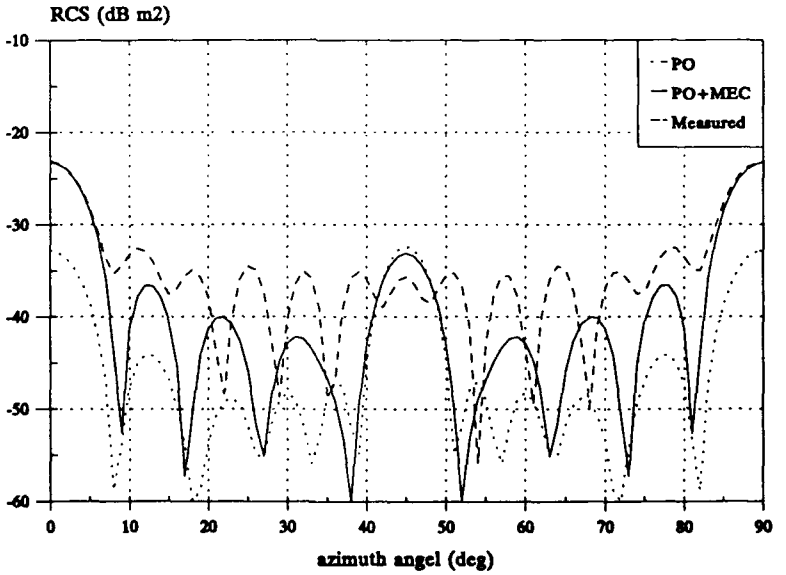

Fig 3.15: *Measured and computed results for the pyramid. Frequency used is 10 GHz, polarisation is H-H.*

From the results presented in fig 3.14 and 3.15 it will be clear that the methods used in this report are completely unable to predict the scattering from this pyramid. The reason for this is not obvious, but there are a few possibilities. Because the peak levels at 0°, 45° and 90° are

predicted quite well, it is not likely that one of the methods used fails for this object. It is more probable, however, that different phenomena, like the surface travelling wave, for instance, play an important role in the case of scattering by a pyramid. Another possibility might be the fact that the size of the pyramid is not sufficient to allow high-frequency approximations to be used. It cannot be stated with certainty what the reason for the discrepancy is, but in my personal opinion the latter reason is the more obvious one.

3.5 Circular cylinder

The cylinder used has a length of 17.178 cm (7") and a radius of 7.1 cm (2.8"). It is located along the z-axis with its centre at the origin of the co-ordinate axes. Like in the case of the square rod, see section 3.2, the cylinder was located differently during the measurements, but again this does not pose a noticeable difference.

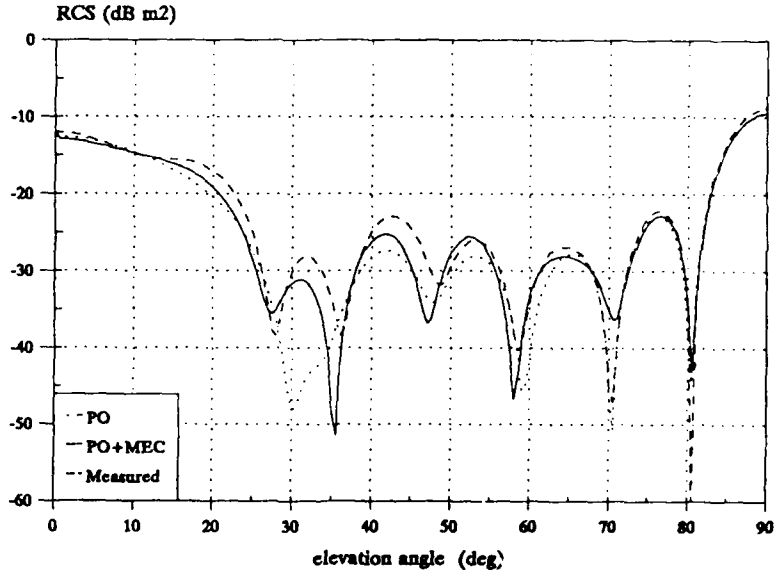

Fig 3.16: Measured and computed results for the circular cylinder. Frequency used is 5 GHz, polarisation is V-V.

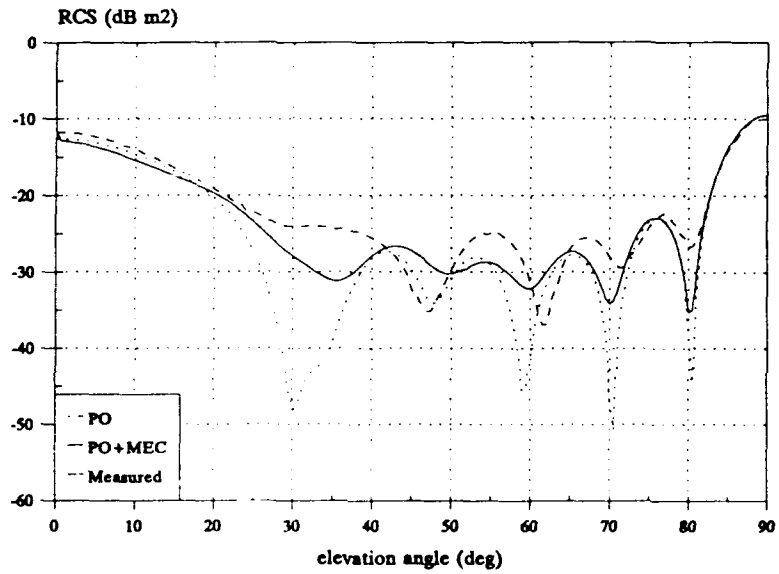

Fig 3.17: *Measured and computed results for the circular cylinder. Frequency used is 5 GHz, polarisation is H-H.*

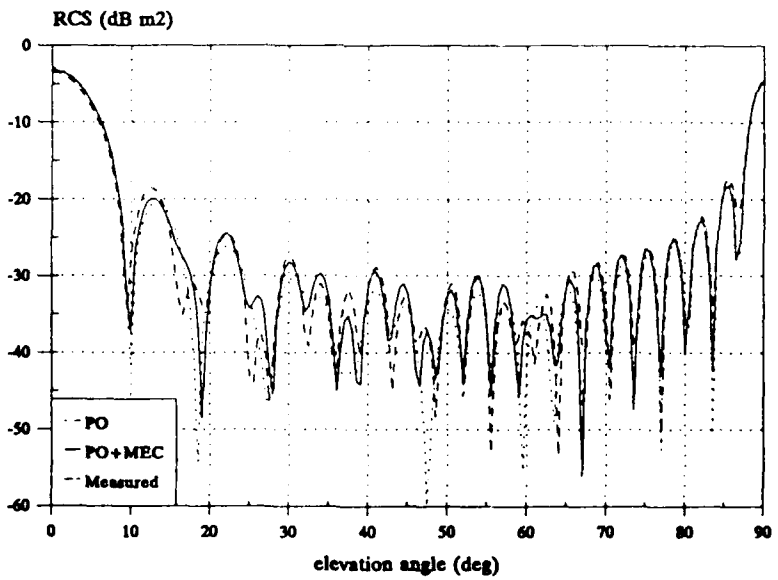

Fig 3.18: *Measured and computed results for the circular cylinder. Frequency used is 15 GHz, polarisation is V-V.*

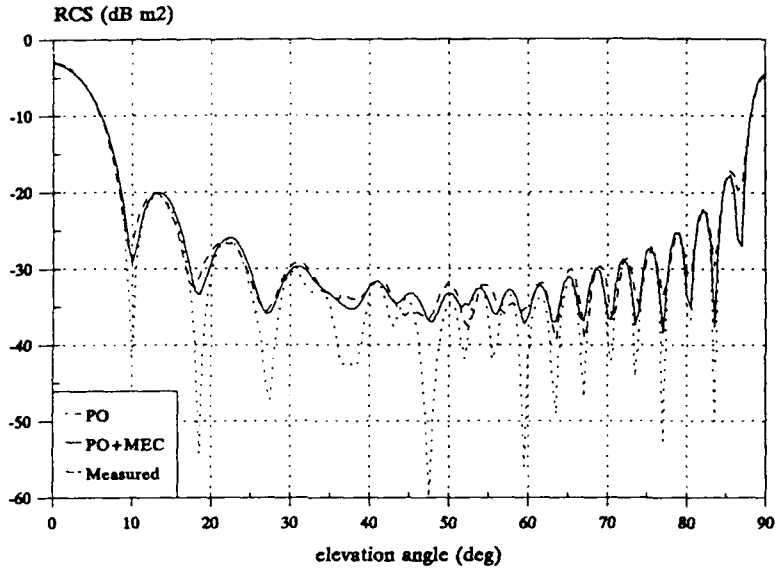

Fig 3.19: *Measured and computed results for the circular cylinder. Frequency used is 15 GHz, polarisation is H-H.*

The circular cylinder displays a similar behaviour as does the square rod. This is not surprising because the dimensions are closely related. The MEC improves the PO prediction and even for the lower frequency the total result agrees well with the measured data, although the results for the square rod at the lower frequency are better. Also the more pronounced lobing structure for the 15 GHz V-V results are predicted to a reasonable degree of accuracy.

3.6 Summary of the comparisons

It is not a trivial or simple conclusion that can be drawn from the large amount of comparisons presented in this chapter. For the square plate, for vertical polarisation, the improvement of PO by MEC is very good, whereas for horizontal polarisation it is rather poor. For other shapes the difference between the two polarisations is not as pronounced and in general the results of measurement and computation are in agreement to a comfortable level.

Bad extremities are displayed by the equilateral plate and the pyramid. Possible reasons for this are given in sections 3.3 and 3.4.

The main concern at this moment is the fact that, for simple shapes, the surface travelling wave can give an important contribution to the total scattering. It is strongly believed that an implementation of this scattering phenomenon will improve most of the results given in this chapter.

Finally a word on the choice of the objects used for the comparisons. This selection is made out of a much larger set. The reason that these specific objects are chosen is that they display the widest possible variety of shapes, like straight , slanted and sharp edges as well as flat and curved surfaces. This way a fair and objective judgement of the method can be made, see section 4.1.

4 CONCLUSIONS AND RECOMMENDATIONS

4.1 Conclusions

The MEC was derived in the same rigorous way Michaeli did. The expressions found reflect the non-uniform currents only and therefore the computed scattered field is only the diffracted field. The advantage of this, over an expression reflecting the total currents, is the capability to investigate the contribution of the diffracted field to the total scattered field.
The method is made almost completely uniform in that the last remaining singularities, at the shadow and reflection boundaries, are removed as well. These singularities prevented the method to be used at these aspect angles and were not treated in literature before. The only remaining singularity is the so-called Ufimtsev singularity, occurring when one wants to compute the diffracted field in the direction of the grazing diffracted ray and the incident field comes from outside the wedge. This situation only occurs in forward scattering.
From the results shown in chapter 3 it can be concluded that the method is capable of computing the diffracted field by any edge for all directions of incidence and observation, excluding the one mentioned above, and that such a computation can provide a valuable supplement to for instance PO. The method seems to provide better results for fields incident perpendicularly to an edge than otherwise, which is something that needs more research.
Furthermore it is shown that the combination of PO and MEC, although physically only valid in the high-frequency region, provide valid results for simple objects as small as only a few wavelengths. The polarisation dependent scattering is not modelled very well by the MEC, although better than by PO alone, which completely ignores this dependency. A method to improve on this is mentioned in section 4.2.

4.2 Recommendations

Because of the problems that the MEC encounters at grazing incidence for parallel polarisation it is strongly recommended that the method will be adjusted or extended in order to overcome these failures. This can be done by adding the capability to compute multiple diffraction which accounts for the interaction of the diffracted field with another edge. In general this is not possible by applying the MEC again at the other edge, because the diffracted fields do not always display a ray-optical behaviour at the other edge which is a necessary requirement for the application of the MEC. Other diffraction theories have the same problems and in the case of the UTD this was overcome by a spectral analysis of the diffracted field. Although this hasn't been done with the MEC yet, it seems feasible to perform such a spectral analysis with the MEC as well.
This interaction of the diffracted fields with other edges is a simulation of the surface travelling wave, the high-frequency phenomenon that causes the discrepancies of any diffraction theory at low grazing angles.
When such an improvement is implemented the combination of PO and MEC can be expected to be able to give accurate results for all kinds of objects in a large frequency region. Especially the RCS prediction of not to complex, low-RCS objects will benefit from this.

REFERENCES

[1] E.F. Knott, J.F. Shaeffer and M.T. Tuley, "Radar Cross Section, its Prediction, Measurement and Reduction", Artech House, 1985

[2] R.F. Millar, "An Approximate Theory of the Diffraction of an Electromagnetic Wave by an Aperture in a Plane Screen", Proc. Inst. Elec. Eng., Vol. 103 (pt C), pp 177-185, March 1956.

[3] R.F. Millar, "The Diffraction of an Electromagnetic Wave by a Circular Aperture", Proc. Inst. Elec. Eng., Vol. 104 (pt C), pp 87-95, March 1957.

[4] R.F. Millar, "The Diffraction of an Electromagnetic Wave by a Large Aperture", Proc. Inst. Elec. Eng., Vol. 104 (pt C), pp 240-250, September 1957.

[5] C.E Ryan jr. and L. Peters jr., Evaluation of Edge-diffracted Fields Including Equivalent Currents for teh Caustic Regions", IEEE Trans. on Ant. and Prop., Vol AP-17, pp 292-299, May 1969 (see also correction Vol. AP-18, p 275).

[6] E.F. Knott and T.B.A Senior, "Comparison of Three High-frequency Diffraction Techniques", Proc. IEEE, Vol. 62, pp. 1468-1474, Nov 1974.

[7] F.A. Sikta, W.D. Burnside, T. Chu and L. Peters jr., "First-Order Equivalent Current and Corner Diffraction Scattering from Flat Plate Structures", IEEE Trans. on Ant. and Prop., Vol. AP-31, No. 4, pp. 584-589, July 1983.

[8] A. Michaeli, "Equivalent Edge Currents for Arbitrary Aspects of Observation", IEEE Trans. on Ant. and Prop., Vol. AP-23, No. 3, pp. 252-258, March 1983.

[9] A. Michaeli, "Elimination of Infinities in Equuivalent Edge Currents, Part 1: Fringe Current Components", IEEE Trans. on Ant. and Prop., Vol. AP-34, No. 7, pp. 912-918, July 1986.

[10] R.A. Shore and A.D. Yaghjian, "Incremental Diffraction Coefficients for Planar Surfaces", IEEE Trans. on Ant. and Prop., Vol. TAP-36, No. 1, pp. 55-70, Jan. 1988.

[11] E.F. Knott, "The Relationship between Mitzner's ILDC and Michaeli's Equivalent Currents", IEEE Trans. on Ant. and Prop., Vol. AP-33, No. , pp. 112-114, 1985.

[12] D.W. Duan, Y. Rahmat-Samii and J.P. Mahon, "Scattering from a Circular Disk: A Comparative Study of PTD and GTD Techniques", Proc. IEEE, pp. 1472-1480, Oct. 1991.

[13] G.L. James, "Geometrical Theory of Diffraction for Electromagnetic Waves", Hertfordshire, England, Peter Peregrinus, 1976.

[14] G.T. Ruck, D.E. Barrick, W.D. Stuart and C.K. Krichbaum, "Radar Cross Section Handbook", Vol. 1, New York, Plenum Press, 1970.

H.R. van Es
(Group leader)

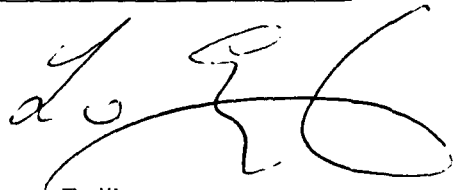

L.J. van Ewijk
(Author)

APPENDIX A: DERIVATION OF THE EQUIVALENT CURRENTS

By comparing eq (2) and (4) in the main text we see that:

$$\begin{aligned}\left[I_e(\hat{k}_s x(\hat{k}_s x\hat{t})) - \sqrt{\frac{\varepsilon}{\mu}} I_m(\hat{t} x\hat{k}_s)\right]\psi_e &= \int (\hat{k}_s x(\hat{k}_s x\hat{J}))\psi_e e^{ik(\vec{\sigma}_n\cdot\hat{k}_s)}dx_n \\ \left[I_e(\hat{k}_s x(\hat{k}_s x\hat{t})) - \sqrt{\frac{\varepsilon}{\mu}} I_m(\hat{t} x\hat{k}_s)\right] &= \hat{k}_s x\left[\hat{k}_s x\int \vec{J}_e e^{ik(\vec{x}_n\cdot\hat{k}_s)}dx_n\right]\end{aligned} \tag{A.1}$$

By taking the scalar product of eq (A.1) with $k_S x(k_S xt)$ or $(k_S xt)$ we arrive at an expression for I_e or I_m respectively:

$$\begin{aligned}I_e &= \frac{1}{\sin^2(\theta_s)}\hat{k}_s\cdot\left[(\hat{t} x\hat{k}_s)x\int \vec{J}(\sigma\sin(\theta_1),\sigma\cos(\theta_1))e^{ik(\vec{\sigma}\cdot\hat{k}_s)}d\sigma\right] \\ I_m &= \frac{1}{\sin^2(\theta_s)}\sqrt{\frac{\mu}{\varepsilon}}\hat{t}\cdot\left[\hat{k}_s x\int \vec{J}(\sigma\sin(\theta_1),\sigma\cos(\theta_1))e^{ik(\vec{\sigma}\cdot\hat{k}_s)}d\sigma\right]\end{aligned} \tag{A.2}$$

So the evaluation of I_e and I_m can now be completed by an asymptotic end-point evaluation of the current integral in eq's (A.2) for a canonical wedge problem. When we use the following property of the 3-dimensional solution of the canonical wedge problem, see James [13]:

$$\vec{J}(x,z) = \vec{J}(x,0)e^{-ikz\cos(\theta_1)} \tag{A.3}$$

and evaluate the vector products in eq (A.2) we arrive at:

$$\begin{aligned}I_e &= \int\left[J_z - \frac{\cos(\theta_2)\cos(\varphi_2)}{\sin(\theta_2)}J_x\right]e^{ik(\vec{\sigma}\hat{k}_s-\cos^2(\theta_1))}\sin(\theta_1)d\sigma \\ I_m &= -Z\frac{\sin(\varphi_2)}{\sin(\theta_2)}\int J_x e^{ik(\vec{\sigma}\hat{k}_s-\cos^2(\theta_1))}\sin(\theta_1)d\sigma\end{aligned} \tag{A.4}$$

The currents, J, in these expressions are supposed to be the fringe currents, or non-uniform currents, only and not the total surface currents and are evaluated at $(\sigma\sin(\theta_1), 0)$.
We can, in the usual way, express the currents as the cross product of the surface normal, (0, 1, 0), and the magnetic field at the surface. Then, with Maxwell's equations and the expressions for the incident fields at the surface:

$$\begin{aligned}\vec{\nabla}x\vec{E} &= -i\omega\mu\vec{H}\\ \vec{\nabla}x\vec{H} &= i\omega\varepsilon\vec{E}\end{aligned} \tag{A.5}$$

and

$$\begin{aligned}\vec{E}_i &= \vec{E}_{0i}e^{-ik(\hat{k}_i\cdot\vec{r})} = \vec{E}_{0i}e^{-ik(x\sin(\theta_i)\cos(\varphi_i)+z\cos(\theta_i))}\\ \vec{H}_i &= \vec{H}_{0i}e^{-ik(\hat{k}_i\cdot\vec{r})} = \vec{H}_{0i}e^{-ik(x\sin(\theta_i)\cos(\varphi_i)+z\cos(\theta_i))}\end{aligned} \tag{A.6}$$

we can easily find an expression for H_X as function of E_Z and H_Z, which is needed in the expression for the current. This equation is:

$$H_x = \frac{1}{ik\sin^2(\theta_i)}\left[-\sqrt{\frac{\varepsilon}{\mu}}\frac{\partial E_z}{\partial y}+\cos(\theta_i)\frac{\partial H_z}{\partial x}\right] \tag{A.7}$$

From James we now use the canonical wedge solution to relate E_Z and H_Z to E_{iZ} and H_{iZ} as:

$$\begin{aligned}E_z &= E_{0iz}\left[u(X,\psi-\varphi_i)-u(X,\psi+\varphi_i)\right]\\ H_z &= H_{0iz}\left[u(X,\psi-\varphi_i)+u(X,\psi+\varphi_i)\right]\end{aligned} \tag{A.8}$$

with

$$X = k\sigma\sin^2(\theta_i)$$

$$u(X,\phi) = \frac{1}{2\pi iN}\int_\Gamma \frac{\sin(\frac{\xi}{N})e^{iX\cos(\xi)}}{\cos(\frac{\xi}{N})-\cos(\frac{\phi}{N})}d\xi$$

and ϕ the polar angle of the field point in the xy plane, so for our purposes ϕ=0.
By substituting eq (A.7), (A.8) and the expression of the surface current in terms of the magnetic field in (A.4) we get the expressions for the electric and magnetic equivalent currents. This will be done first for the magnetic current.
From the definition of u following eq (A.8) we see that $u(X,-\phi)=u(X,\phi)$ because ϕ is only present in the cos term. Also, with the definition of X, we can change to X as the variable of integration. This yields:

$$I_m = -Z\frac{\sin(\varphi_2)}{\sin(\theta_2)}\int H_{0iz}[u(X,-\varphi_i)+u(X,\varphi_i)]\sin(\theta_i)e^{ik\sigma(\hat{\sigma}\cdot\hat{k}_i-\cos^2(\theta_i))}d\sigma \tag{A.9}$$

$$I_m = -\frac{2ZH_{0iz}\sin(\varphi_2)}{k\sin(\theta_1)\sin(\theta_2)}\int u(X,\varphi_1)e^{i\mu X} \tag{A.10}$$

with μ following from the comparison of eq (A.9) and (A.10) as:

$$\begin{aligned}\mu &= \frac{k\sigma(\hat{\sigma}\cdot\hat{k}_s - \cos^2(\theta_1))}{k\sigma\sin^2(\theta_1)} \\ &= \frac{\sin(\theta_1)\sin(\theta_2)\cos(\varphi_2)+\cos(\theta_1)\cos(\theta_2)-\cos^2(\theta_1)}{\sin^2(\theta_1)}\end{aligned} \tag{A.11}$$

The derivation of I_e is a little more complex, but we can make use of the expression for I_m from eq (A.10).
In terms of the surface currents we have:

$$\begin{aligned}I_e &= \int J_z e^{ik\sigma(\hat{\sigma}\cdot\hat{k}_s-\cos^2(\theta_1))}\sin(\theta_1)d\sigma \\ &-\frac{\cos(\theta_2)\cos(\varphi_2)}{\sin(\theta_2)}\int J_x e^{ik\sigma(\hat{\sigma}\cdot\hat{k}_s-\cos^2(\theta_1))}\sin(\theta_1)d\sigma\end{aligned} \tag{A.12}$$

The second term, including the minus sign, is equal to $\cos(\varphi_2)/(Z\tan(\theta_2))\ I_m$, with I_m as given in eq (A.10). We therefore only have to elaborate the first term in eq (A.12). We know that J_z can be expressed in terms of H_x and with eq (A.7) and (A.8) in terms of E_{iz} and H_{iz}. We then find for the z-component of the surface current:

$$\begin{aligned}J_z = -\frac{1}{ik\sin^2(\theta_1)}\{&-\sqrt{\frac{\varepsilon}{\mu}}E_{0iz}[\frac{\partial u(X,-\varphi_1)}{\partial y}-\frac{\partial u(X,\varphi_1)}{\partial y}] \\ &+\cos(\theta_1)H_{0iz}[\frac{\partial u(X,-\varphi_1)}{\partial x}+\frac{\partial u(X,\varphi_1)}{\partial x}]\}\end{aligned} \tag{A.13}$$

Because $X=k\sigma\sin^2(\theta_1)$ and $x=\sigma\sin(\theta_1)$ we can replace dx by $dX/(k\sin(\theta_1)$ and also, from geometrical point of view:

$$\begin{aligned}\frac{\partial u}{\partial y} &= \frac{1}{\rho}\frac{\partial u}{\partial\varphi_1} \\ &= \frac{k\sin(\theta_1)}{X}\frac{\partial u}{\partial\varphi_1}\end{aligned}$$

From the definition of u, following eq (A.8) we can deduct:

$$\left.\frac{\partial u}{\partial \phi}\right|_{\phi=-\varphi_1} = \left.\frac{\partial u}{\partial \phi}\right|_{\phi=\varphi_1}$$

All this substituted in eq (A.13) gives:

$$J_z = -\frac{1}{ik\sin^2(\theta_1)}\left(\sqrt{\frac{\varepsilon}{\mu}}2E_{0iz}\frac{k\sin(\theta_1)}{X}\frac{\partial u(X,\varphi_1)}{\partial \varphi_1} + 2H_{0iz}k\sin(\theta_1)\cos(\theta_1)\frac{\partial u(X,\varphi_1)}{\partial X}\right) \tag{A.14}$$

So we have for the first term of eq (A.12):

$$I_{e1} = \frac{2i\sqrt{\frac{\varepsilon}{\mu}}E_{0iz}}{k\sin^2(\theta_1)}\int\frac{1}{X}\frac{\partial u}{\partial \varphi_1}e^{iX\mu}dX + \frac{2iH_{0iz}\cos(\theta_1)}{k\sin^2(\theta_1)}\int\frac{\partial u}{\partial X}e^{iX\mu}dX \tag{A.15}$$

with μ as defined in eq (A.11).
The second term of eq (A.12) follows easily from eq (A.10), see text following eq (A.12) and reads:

$$\begin{aligned} I_{e2} &= -\frac{\cos(\theta_2)}{Z\tan(\varphi_2)}\frac{2H_{0iz}\sin(\varphi_2)}{k\sin(\theta_1)\sin(\theta_2)}\int u(X,\varphi_1)e^{iX\mu}dX \\ &= -\frac{2H_{0iz}\cos(\varphi_2)\cos(\theta_2)}{k\sin(\theta_1)\sin(\theta_2)}\int u(X,\varphi_1)e^{iX\mu}dX \end{aligned} \tag{A.16}$$

We now have found the expressions for the electric and magnetic equivalent currents in eq (A.15)+(A.16) and (A.10) respectively.
The integrals in these equations will be evaluated by using the method of stationary phase, resulting in their asymptotic end-point value at the edge [8]. The function u is defined as a contour integral in the complex plane, see figure A.1 for the contour.
From eq (A.10), (A.15), (A.16) and the definition of u following eq (A8) we see that we must compute three different contour integrals. We will do this starting with the one that is given in eq (A.10). When we substitute the definition of u in this equation and omit the term in front of the integral for now, we have:

$$u = \int \frac{1}{2\pi i N} \int_{\Gamma} \frac{\sin(\frac{\xi}{N}) e^{iX(\cos(\xi)+\mu)}}{\cos(\frac{\xi}{N}) - \cos(\frac{\phi}{N})} d\xi dX \qquad (A.17)$$

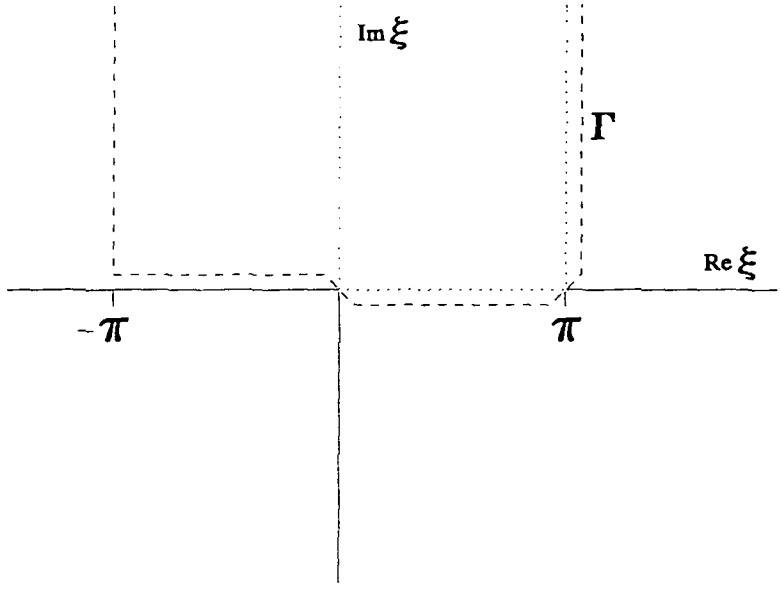

Fig A.1: *The contour of integration for the canonical wedge problem, denoted by the dashed line, when only the fringe currents are involved.*

The contour shown in figure A.1 is the same as the distorted contour that Michaeli used in his derivation of the total equivalent currents. The exponential term converges on the contour when X approaches infinity for every ξ, therefore we may reverse the order of integration, see [8].
We integrate eq (A.17) to X, using only the value at the edge, and arrive at:

$$u = \frac{1}{2\pi i N} \int_{\Gamma} \frac{i \sin(\frac{\xi}{N})}{\left[\cos(\frac{\xi}{N}) - \cos(\frac{\varphi_1}{N})\right] \cos(\xi + \mu)} d\xi \qquad (A.18)$$

When the contour is now closed at infinity, this integral can be computed with the residue theorem.
The poles of the function are located at the positive x-axis and are given by:

$$\cos(\frac{\xi_n}{N}) = \cos(\frac{\varphi_1}{N}) \qquad (A.19)$$

and

$$\begin{aligned}\cos(\xi_x) &= -\mu \\ \xi_x &= \pi - \arccos(\mu) \\ &= \pi - \alpha\end{aligned} \tag{A.20}$$

The residues in the poles given by eq (A.19) can be calculated with:

$$\mathrm{Res} = \lim_{\xi \to \xi_n} (\xi - \xi_n) \frac{i \sin(\frac{\xi}{N})}{-2 \sin(\frac{\xi + \varphi_1}{2N}) \sin(\frac{\xi - \varphi_1}{2N})} \tag{A.21}$$

which follows from elementary goniometric relations and the solution of eq (A.19). The residue at the pole given by eq (A.20) is:

$$\begin{aligned}\mathrm{Res} &= \lim_{\xi \to \xi_x} (\xi - \xi_x) \frac{i \sin(\frac{\xi}{N})}{[\cos(\frac{\xi}{N}) - \cos(\frac{\varphi_1}{N})](-2 \sin(\frac{1}{2(\xi + \xi_x)}) \sin(\frac{1}{2(\xi - \xi_x)}))} \\ &= \frac{-i \sin(\frac{\pi - \alpha}{N})}{[\cos(\frac{\pi - \alpha}{N}) \cos(\frac{\varphi_1}{N})] \sin(\alpha)}\end{aligned} \tag{A.22}$$

According to the residue theorem the integral evaluates as $2\pi i$ times the sum of the residues when the direction of the contour is counter clockwise around the poles, which is the case here. So the final result for this integral (eq (A.18) can now be written as:

$$u = -\frac{1}{N} \{ \frac{N}{\cos(\varphi_1) + \mu} + \frac{\sin(\frac{\pi - \alpha}{N})}{\cos(\frac{\pi - \alpha}{N}) - \cos(\frac{\varphi_1}{N})} \frac{1}{\sin(\alpha)} \} \tag{A.23}$$

The remaining two integrals are computed in the same manner.
The differentiation of u to X in eq (A.15) can be performed without difficulty and results in an equation that resembles eq (A.17) very much. This equation can be treated exactly as is done above and results in:

$$u = \int \frac{\partial u}{\partial X} e^{iX\mu} dX$$

$$= -\frac{1}{N}\frac{\cos(\alpha)}{\sin(\alpha)}\frac{\sin(\frac{\pi-\alpha}{N})}{\cos(\frac{\pi-\alpha}{N})-\cos(\frac{\varphi_1}{N})} \qquad (A.24)$$

The integral with the differentiation of u to φ can be solved if the term with this differentiation is first integrated by parts [8], which results in:

$$\frac{1}{X}\frac{\partial u}{\partial \varphi_1} = -\frac{\sin(\frac{\varphi_1}{N})}{2\pi i N}\int_r \frac{\sin(\xi)e^{iX\cos(\xi)}}{\cos(\frac{\xi}{N})-\cos(\frac{\varphi_1}{N})} d\xi \qquad (A.25)$$

With this substitution we can find:

$$u = \int \frac{1}{X}\frac{\partial u}{\partial \varphi_1} e^{iX\mu} d\xi dX$$

$$= -\frac{1}{N}\frac{\sin(\frac{\varphi_1}{N})}{\cos(\frac{\pi-\alpha}{N})-\cos(\frac{\varphi_1}{N})} \qquad (A.26)$$

The expressions for the integrals are now known, so they can be used in the expressions for the equivalent electric and magnetic currents. So we substitute eq (A.24) in (A.10) and (A.24), (A.25) and (A.26) in (A.15) and (A.16) and sum the last two, resulting in:

$$I_m = \frac{2iZH_{0iz}\sin(\varphi_2)}{Nk\sin(\theta_1)\sin(\theta_2)}\left[\frac{NU(\pi-\varphi_1)}{\cos(\varphi_1)+\mu_1} + \frac{\sin(\frac{\pi-\alpha_1}{N})}{\cos(\frac{\pi-\alpha_1}{N})-\cos(\frac{\varphi_1}{N})}\frac{1}{\sin(\alpha_1)}\right] \qquad (A.27)$$

and

$$I_e = \frac{2iE_{0iz}}{NkZ\sin^2(\theta_1)}\left[\frac{N\sin(\varphi_1)U(\pi-\varphi_1)}{\cos(\varphi_1)+\mu_1} - \frac{\sin(\frac{\varphi_1}{N})}{\cos(\frac{\pi-\alpha_1}{N})-\cos(\frac{\varphi_1}{N})}\right]$$
$$+\frac{2iH_{0iz}\cos(\theta_1)}{Nk\sin^2(\theta_1)}\left[\frac{\cos(\varphi_1)U(\pi-\varphi_1)}{\cos(\varphi_1)+\mu_1} - \frac{\sin(\frac{\pi-\alpha_1}{N})}{\cos(\frac{\pi-\alpha_1}{N})-\cos(\frac{\varphi_1}{N})}\frac{\mu_1}{\sin(\alpha_1)}\right]$$
$$+\frac{2iH_{0iz}\cos(\varphi_2)}{Nk\sin(\theta_1)\tan(\theta_2)}\left[\frac{NU(\pi-\varphi_1)}{\cos(\varphi_1)+\mu_1} + \frac{\sin(\frac{\pi-\alpha_1}{N})}{\cos(\frac{\pi-\alpha_1}{N})-\cos(\frac{\varphi_1}{N})}\frac{1}{\sin(\alpha_1)}\right]$$

(A.28)

Eq (A.27) and (A.28) give the equivalent currents flowing on face 1 of the edge. The currents on face 2 can be found by performing the following substitutions in these equations:

$$\begin{aligned}\varphi_i &= N\pi - \varphi_i \\ \theta_i &= \pi - \theta_i \\ z &= -z\end{aligned} \qquad \text{(A.29)}$$

We can then determine the equivalent currents on the second face of the wedge and subtract this from the value of the first face in order to find the complete expressions for the equivalent currents. These expressions are given in the main text, in eq's .(5) and (6).

APPENDIX B: REMOVING SINGULARITIES FROM THE EQUIVALENT CURRENTS

In this chapter we will show how the diffraction coefficients, derived in the main text, can be made uniform. The way they are given now still contains non-uniformities that become apparent at, for instance, the optical boundaries. Although this can be circumvented quite easily in a computer program, it is far more appealing to have expressions that can be used for every angle of incidence and observation.

This is done in this chapter by determining the limiting value of every expression that becomes singular. In the computer program, where these coefficients are used, one must switch between the original expression and the limiting one when an optical boundary is approached. Because the original expressions only become singular at the optical boundary itself, the mentioned switch can be made as close as 0.01 or 0.001 degree from the boundary, depending on the numerical accuracy of the computer used.

First the expressions for the diffraction coefficients are given again and the singularities are pointed out. Further we look more specifically at the terms that actually become singular. In the main text we can find D_m, D_e and D_x and slightly rewritten they read:

$$D_m = \frac{\sin(\varphi_2)U(\pi-\varphi_1)}{\cos(\varphi_1)+\mu_1} + \frac{\sin(N\pi-\varphi_2)U((1-N)\pi+\varphi_1}{\cos(N\pi-\varphi_1)+\mu_2} + \frac{\sin(\frac{\pi-\alpha_1}{N})}{N[\cos(\frac{\pi-\alpha_1}{N})-\cos(\frac{\varphi_1}{N})]}\frac{\sin(\varphi_2)}{\sin(\alpha_1)} + \frac{\sin(\frac{\pi-\alpha_2}{N})}{N[\cos(\frac{\pi-\alpha_2}{N})+\cos(\frac{\varphi_1}{N})]}\frac{\sin(N\pi-\varphi_2)}{\sin(\alpha_2)} \tag{B.1}$$

$$D_e = -\frac{\sin(\varphi_1)U(\pi-\varphi_1)}{\cos(\varphi_1)+\mu_1} - \frac{\sin(N\pi-\varphi_1)U((1-N)\pi+\varphi_1)}{\cos(N\pi-\varphi_1)+\mu_2} - \frac{\sin(\frac{\varphi_1}{N})}{N[\cos(\frac{\pi-\alpha_1}{N})-\cos(\frac{\varphi_1}{N})]} - \frac{\sin(\frac{\varphi_1}{N})}{N[\cos(\frac{\pi-\alpha_2}{N})+\cos(\frac{\varphi_1}{N})]} \tag{B.2}$$

$$
\begin{aligned}
D_x = & \frac{1}{\tan(\theta_1)}\left[\frac{\cos(\varphi_1)U(\pi-\varphi_1)}{\cos(\varphi_1)+\mu_1} - \frac{\cos(N\pi-\varphi_1)U((1-N)\pi+\varphi_1}{\cos(N\pi-\varphi_1)+\mu_2}\right] \\
& + \frac{1}{\tan(\theta_2)}\left[\frac{\cos(\varphi_2)U(\pi-\varphi_1)}{\cos(\varphi_1)+\mu_1} - \frac{\cos(N\pi-\varphi_2)U((1-N)\pi+\varphi_1}{\cos(N\pi-\varphi_1)+\mu_2}\right] \\
& - \frac{\sin(\frac{\pi-\alpha_1}{N})}{N\left[\cos(\frac{\pi-\alpha_1}{N})-\cos(\frac{\varphi_1}{N})\right]\sin(\alpha_1)}\left[\frac{\mu_1}{\tan(\theta_1)} - \frac{\cos(\varphi_2)}{\tan(\theta_2)}\right] \\
& + \frac{\sin(\frac{\pi-\alpha_2}{N})}{N\left[\cos(\frac{\pi-\alpha_2}{N})+\cos(\frac{\varphi_1}{N})\right]\sin(\alpha_2)}\left[\frac{\mu_2}{\tan(\theta_1)} - \frac{\cos(N\pi-\varphi_2)}{\tan(\theta_2)}\right]
\end{aligned}
\tag{B.3}
$$

Starting with the expression for D_m we can see that this coefficient is singular when:

$$
\begin{aligned}
&\cos(\varphi_1) = -\mu_1 \\
&\cos(N\pi-\varphi_1) = -\mu_2 \\
&\cos(\frac{\pi-\alpha_1}{N}) = \cos(\frac{\varphi_1}{N}) \\
&\cos(\frac{\pi-\alpha_2}{N}) = -\cos(\frac{\varphi_1}{N})
\end{aligned}
\tag{B.4}
$$

From these equations we can find the values of α_1 and α_2 for the singular directions:

$$
\begin{aligned}
&\alpha_1 = \pi-\varphi_1 \qquad \vee\ \pi+\varphi_1 \\
&\alpha_2 = \pi-N\pi+\varphi_1 \vee\ \pi+N\pi-\varphi_1
\end{aligned}
\tag{B.5}
$$

The values of α_1 in the first line cause the terms for face 1 to be singular and the values of α_2 in the second line cause the terms for face 2 to be singular.
When the observation direction is on the Keller cone of directions and we express φ_2 in terms of α_1 or α_2, we see that these singular directions coincide with the reflection and shadow boundary of face 1 and face 2 respectively. In general, however, these singularities exist outside the Keller cone as well, so we don't make any a priori statement about φ_2.
The components of D_m that become singular for $\alpha_1 = \pi\pm\varphi_1$ are taken together and we then try to determine the value of this combination when α_1 approaches one of these values infinitely close. These terms are:

$$t_1 = \frac{\sin(\frac{\pi-\alpha_1}{N})\sin(\varphi_2)}{N\sin(\alpha_1)[\cos(\frac{\pi-\alpha_1}{N})-\cos(\frac{\varphi_1}{N})]} + \frac{\sin(\varphi_2)}{\cos(\varphi_1)+\cos(\alpha_1)} \qquad (B.6)$$

When we substitute $\alpha_1 = \pi-\varphi_1+\delta$ in equation (B.6) and take the limit for δ approaching 0 we arrive at:

$$t'_1 = \lim_{\delta\to 0}\left[\frac{\sin(\frac{\varphi_1-\delta}{N})\sin(\varphi_2)}{N\sin(\varphi-\delta)\left[\cos(\frac{\varphi_1-\delta}{N})-\cos(\frac{\varphi_1}{N})\right]} + \frac{\sin(\varphi_2)}{\cos(\varphi_1)-\cos(\varphi_1-\delta)}\right] \qquad (B.7)$$

When the sum of the two cosines in the denominator is expanded we get terms that contain $\delta/2$. For later use we therefore introduce these same terms in the numerator as well in the following way:

$$t'_1 = \lim_{\delta\to 0}\left\{\frac{\sin(\varphi_2)}{\sin(\varphi_1-\delta)}\left[\frac{\sin(\frac{\varphi_1-\delta/2}{N}-\frac{\delta/2}{N})}{2N\sin(\frac{\varphi_1-\delta/2}{N})\sin(\frac{\delta/2}{N})} - \frac{\sin(\varphi_1-\delta/2-\delta/2)}{2\sin(\varphi_1-\delta/2)\sin(\delta/2)}\right]\right\} \qquad (B.8)$$

We now expand the terms in the numerator and divide equals terms out so that we reach:

$$t'_1 = \lim_{\delta\to 0}\left\{\frac{\sin(\varphi_2)}{\sin(\varphi_1-\delta)}\left[\frac{\cos(\frac{\delta/2}{N})}{2N\sin(\frac{\delta/2}{N})} - \frac{\cos(\frac{\varphi_1-\delta/2}{N})}{2N\sin(\frac{\varphi_1-\delta/2}{N})} - \frac{\cos(\varphi_1-\delta/2)}{2\sin(\varphi_1-\delta/2)}\right]\right\} \qquad (B.9)$$

In the limit we can simply set δ equal to 0 in almost all terms, except in those where the term would become infinite by doing so. This happens in the two terms with $\sin(\delta/x)$ in the denominator. For δ very small, however, we can replace sin by its argument and cos by 1. When we do this we see that the singular terms cancel exactly and we get for the limit:

$$t'_1 = \frac{\sin(\varphi_2)}{\sin(\varphi_1)}\left\{\frac{-1}{2N\tan(\frac{\varphi_1}{N})} + \frac{1}{2\tan(\varphi_1)}\right\} \tag{B.10}$$

When $\alpha_1 = \pi+\varphi_1+\delta$ is substituted in eq (B.6) and we follow the same derivation we arrive at exactly the same expression for the combination of the singular terms.
This expression should therefore be used instead of the original one when α_1 is near one of the above mentioned values.
When α_2 is near one of the values given in eq (B.5) we must determine the limit for two different terms and for $\alpha_2 = \pi+N\pi-\varphi_1+\delta$ or $\alpha_2 = \pi-N\pi+\varphi_1+\delta$, with δ approaching 0 in both cases. The singular terms are in this case:

$$t_3 = \frac{\sin(\frac{\pi-\alpha_2}{N})\sin(N\pi-\varphi_2)}{N\sin(\alpha_2)[\cos(\frac{\pi-\alpha_2}{N})+\cos(\frac{\varphi_1}{N})]} + \frac{\sin(N\pi-\varphi_2)}{\cos(N\pi-\varphi_1)+\cos(\alpha_2)} \tag{B.11}$$

By Substituting one of the values of α_2, taking the limit for δ approaching 0, introducing terms with $\delta/2$ in the numerator as before and evaluating the resulting expression we arrive at:

$$t_3 = \frac{\sin(N\pi-\varphi_2)}{\sin(N\pi-\varphi_1)}\left[\frac{1}{2N\tan(\frac{\varphi_1}{N})} + \frac{1}{2\tan(N\pi-\varphi_1)}\right] \tag{B.12}$$

This expression is valid for both values of α_2 that cause these terms to become infinite.
By now we have expressions for all singular terms of D_m, so it is now possible to compute the correct value of this coefficient for every angle of incidence and observation. Following the same procedure for D_e we find for the singular terms of face 1:

$$t_5 = -\frac{\sin(\frac{\varphi_1}{N})}{N[\cos(\frac{\pi-\alpha_1}{N})-\cos(\frac{\varphi_1}{N})]} - \frac{\sin(\varphi_1)}{\cos(\varphi_1)+\cos(\alpha_1)} \tag{B.13}$$

and when the limit is computed this results in:

$$t'_5 = -\frac{1}{2N\tan(\frac{\varphi_1}{N})} + \frac{1}{2\tan(\varphi_1)} \tag{B.14}$$

For face 2 the singular terms are:

$$t_7 = -\frac{\sin(\frac{\varphi_1}{N})}{N[\cos(\frac{\pi-\alpha_2}{N}) + \cos(\frac{\varphi_1}{N})]} - \frac{\sin(N\pi-\varphi_1)}{\cos(N\pi-\varphi_1)+\cos(\alpha_2)} \tag{B.15}$$

and their limits are:

$$t'_7 = \frac{1}{2N\tan(\frac{\varphi_1}{N})} + \frac{1}{2\tan(N\pi-\varphi_1)} \tag{B.16}$$

As possible singular terms in D_x we have for face 1:

$$\begin{aligned} t_9 = &-\frac{\sin(\frac{\pi-\alpha_1}{N})}{N\sin(\alpha_1)\left[\cos(\frac{\pi-\alpha_1}{N}) - \cos(\frac{\varphi_1}{N})\right]}\left[\frac{\cos(\alpha_1)}{\tan(\theta_1)} - \frac{\cos(\varphi_2)}{\tan(\theta_2)}\right] \\ &+ \frac{1}{\cos(\varphi_1)+\cos(\alpha_1)}\left[\frac{\cos(\varphi_1)}{\tan(\theta_1)} + \frac{\cos(\varphi_2)}{\tan(\theta_2)}\right] \end{aligned} \tag{B.17}$$

These terms can be treated similar as D_m and D_e above with only one small difference. In this case we arrive at:

$$t'_9 = \lim_{\delta\to 0}\frac{1}{\sin(\varphi_1-\delta)}\left[\left(\frac{\cos(\frac{\delta/2}{N})}{2N\sin(\frac{\delta/2}{N})}-\frac{\cos(\frac{\varphi_1-\delta/2}{N})}{2N\sin(\frac{\varphi_1-\delta/2}{N})}\right)\left(\frac{\cos(\varphi_1-\delta)}{\tan(\theta_1)}+\frac{\cos(\varphi_2)}{\tan(\theta_2)}\right)\right]$$
$$-\left(\frac{\cos(\delta/2}{2\sin(\delta/2)}-\frac{\cos(\varphi_1-\delta/2)}{2\sin(\varphi_1-\delta/2)}\right)\left(\frac{\cos(\varphi_1)}{\tan(\theta_1)}+\frac{\cos(\varphi_2)}{\tan(\theta_2)}\right) \qquad (B.18)$$

Now those terms with $\sin(\delta/x)$ in the denominator do not cancel out as before. The reason for this is that they are not multiplied by the same factor although in the limit, when δ goes to zero, these factors are equal. When $\cos(\varphi 1-\delta)$ is expanded and the goniometric functions are replaced by their small argument values where appropriate we finally get for this limit:

$$t'_9 = \frac{1}{\sin(\varphi_1)}\left[\frac{\sin(\varphi_1)}{\tan(\theta_1)}+\left(\frac{1}{2\tan(\varphi_1)}-\frac{1}{2N\tan(\frac{\varphi_1}{N})}\right)\left(\frac{\cos(\varphi_1)}{\tan(\theta_1)}+\frac{\cos(\varphi_2)}{\tan(\theta_2)}\right)\right] \qquad (B.19)$$

Again, as we saw before with D_m and D_e, this limit is valid for both singularities.
The singular terms for face 2 are:

$$t_{11} = \frac{\sin(\frac{\pi-\alpha_2}{N})}{N\sin(\alpha_2)\left[\cos(\frac{\pi-\alpha_2}{N})+\cos(\frac{\varphi_1}{N})\right]}\left[\frac{\cos(\alpha_2)}{\tan(\theta_1)}-\frac{\cos(N\pi-\varphi_2)}{\tan(\theta_2)}\right]$$
$$-\frac{1}{\cos(N\pi-\varphi_1)+\cos(\alpha_2)}\left[\frac{\cos(N\pi-\varphi_1)}{\tan(\theta_1)}+\frac{\cos(N\pi-\varphi_2)}{\tan(\theta_2)}\right] \qquad (B.20)$$

and following the same way as above, we find for the limit of these terms approaching one of the optical boundaries:

$$t'_{tt} = -\frac{1}{\sin(N\pi-\varphi_1)}\left[\frac{\sin(N\pi-\varphi_1)}{\tan(\theta_1)}+\left(\frac{1}{2N\tan(\frac{\varphi_1}{N})}+\frac{1}{2\tan(N\pi-\varphi_1)}\right)\left(\frac{\cos(N\pi-\varphi_1)}{\tan(\theta_1)}+\frac{\cos(N\pi-\varphi_2)}{\tan(\theta_2)}\right)\right] \tag{B.21}$$

which is valid at both singular directions.

We have determined the values of all pertinent singular terms in the coefficients D_m, D_e and D_x. These expressions, together with the original ones, can be used to compute the diffraction coefficients for all angles of incidence and observation, with the exception of the Ufimtsev singularity. Whenever the observation direction is chosen such that one of the diffraction coefficients becomes singular one has to use the appropriate limit. A reasonable estimate is to change from one expression to the other at 0.1 degree from the singular direction.

APPENDIX C: COMPUTING THE INVERSE COSINE FOR ALL ARGUMENTS

When computing the inverse of the cosine in the programs that apply the MEC it is possible that the result is a complex number. Not every computer can handle this in a correct manner, so in order to prevent problems we will use an unambiguous expression for this function. Such an expression can easily be derived, as will be shown in this chapter. We start with:

$$\begin{aligned} \alpha &= \arccos(\mu) \\ \mu &= \cos(\alpha) \\ &= \frac{1}{2}\left[e^{i\alpha} + e^{-i\alpha}\right] \end{aligned} \tag{C.1}$$

In the usual way we can express $\sin(\alpha)$ as a sum of exponential functions and combination with the last line of eq (C.1) results in:

$$\begin{aligned} e^{i\alpha} &= \mu + i\sqrt{1-\mu^2} \\ \alpha &= -i\ln\left\{\mu + i\sqrt{1-\mu^2}\right\} \end{aligned} \tag{C.2}$$

As long as μ lies between -1 and 1 the square root in eq (C.2) can be evaluated in a straightforward manner. When the value of μ goes beyond these ....., however, one has to be careful. In accordance with Michaeli [8], we make the following choice for α in those cases:

$$\begin{aligned} \alpha &= -i\ln\left\{\mu + \sqrt{\mu^2-1}\right\}, (1 < \mu) \\ \alpha &= -i\ln\left\{\mu - \sqrt{\mu^2-1}\right\}, (-1 < \mu) \end{aligned} \tag{C.3}$$

Eq (C.2) will be used in the other cases.
With this choice of sign we are assured that for any μ:

$$\sin(\alpha) = \sqrt{1-\mu^2} \tag{C.4}$$

REPORT DOCUMENTATION PAGE
(MOD-NL)

1. DEFENCE REPORT NO. (MOD-NL)	2. RECIPIENT'S ACCESSION NO.	3. PERFORMING ORGANIZATION REPORT NO.
TD94-1395		FEL-94-B195
4. PROJECT/TASK/WORK UNIT NO.	**5. CONTRACT NO.**	**6. REPORT DATE**
9310	-	July 1994
7. NUMBER OF PAGES	**8. NUMBER OF REFERENCES**	**9. TYPE OF REPORT AND DATES COVERED**
43 (incl. 3 appendices, excl. RDP & distribution list)	14	

10. TITLE AND SUBTITLE

Diffraction computation by means of the Method of Equivalent Currents

11. AUTHOR(S)

L.J. van Ewijk

12. PERFORMING ORGANIZATION NAME(S) AND ADDRESS(ES)

TNO Physics and Electronics Laboratory, P.O. Box 96864, 2509 JG The Hague, The Netherlands
Oude Waalsdorperweg 63, The Hague, The Netherlands

13. SPONSORING AGENCY NAME(S) AND ADDRESS(ES)

TNO Physics and Electronics Laboratory, P.O. Box 96864, 2509 JG The Hague, The Netherlands
Oude Waalsdorperweg 63, The Hague, The Netherlands

14. SUPPLEMENTARY NOTES

The classification designation Ongerubriceerd is equivalent to Unclassified, Stg. Confidentieel is equivalent to Confidential and Stg. Geheim is equivalent to Secret.

15. ABSTRACT (MAXIMUM 200 WORDS (1044 BYTE))

In this report the derivation of the Method of Equivalent Currents is given. This method can be used to compute the diffraction of plane waves by edges. A computation of this sort is necessary in addition to a scattering computation using Physical Optics or Geometrical Optics, because these last techniques neglect edge effects by definition. The reason that the Method of Equivalent Currents is chosen is because it is a powerful method, valid at almost all incidence and scattering aspects. Some of the few remaining singularities of the method can be removed in a way described in this report as well.
Some interesting comparisons with measured data will be given in order to show the capabilities and shortcomings of the method.

16. DESCRIPTORS	IDENTIFIERS
Radar Cross Section	Diffraction
Mathematical Model	Method of equivalent currents

17a. SECURITY CLASSIFICATION (OF REPORT)	17b. SECURITY CLASSIFICATION (OF PAGE)	17c. SECURITY CLASSIFICATION (OF ABSTRACT)
Ongerubriceerd	Ongerubriceerd	Ongerubriceerd

18. DISTRIBUTION AVAILABILITY STATEMENT	17d. SECURITY CLASSIFICATION (OF TITLES)
Unlimited	Ongerubriceerd